Colloidal Crystals and Water: Perspectives on Liquid-Solid Nanoscale Phenomena in Wet Particulate Media

Francisco Gallego-Gómez,[a] Víctor Morales-Flórez,[b,c] Miguel Morales,[a] Alvaro Blanco[a] and Cefe López[a]*

[a] *Instituto de Ciencia de Materiales de Madrid (CSIC), c/ Sor Juana Inés de la Cruz 3, 28049 Madrid, Spain.*

[b] *Departamento de Física de la Materia Condensada, Universidad de Sevilla, Av. Reina Mercedes, 41012 Seville, Spain.*

[c] *ICMS (CSIC-US) Av. Américo Vespucio 49, 41092 Seville, Spain.*

Keywords: colloidal crystal; particulate media; wet granular materials; interfacial water; micromechanical properties.

Abstract

Solid colloidal ensembles inherently contain water adsorbed from the ambient moisture. This water, confined in the porous network formed by the building submicron spheres, greatly affects the ensemble properties. Inversely, one can benefit from such influence on collective features to explore the water behavior in such nanoconfinements. Recently, novel approaches have been developed to investigate in-depth where and how water is placed in the nanometric pores of self-assembled colloidal crystals. Here we summarize these advances, along with new ones, that are linked to general interfacial water phenomena like adsorption, capillary forces and flow. Water-dependent structural properties of the colloidal crystal give clues to the interplay between nanoconfined water and solid fine particles that determines the behavior of ensembles. We elaborate on how the knowledge gained on water in colloidal crystals provides new opportunities for multidisciplinary study of interfacial and nanoconfined liquids and their essential role in the physics of utmost important systems such as particulate media.

1. Introduction

The behavior of a liquid interacting with a solid surface [1,] is a fundamental subject for a vast number of phenomena. Topics such as adsorption and condensation [2,3], wetting and capillarity [4,5], or liquid-mediated forces [6–78] rely on the physics of liquid-solid interfaces at the smallest scales and are critical for many natural processes in e.g. geology [9], biology [10,11] or meteorology [12]. Nowadays, such phenomena become ever more important in scientific and technological fields, the more, the smaller the relevant scales at play. Nanofluidics [13,14], microseparation [15,16], super liquid-repellency and superwettability [17,18], confined liquids [19,20] and nanotribology [21,22] are only some related issues of significance in current nanomaterials science. However, despite its importance, the behavior of interfacial liquids is still far from being well understood, especially in confined environments.

In turn, the properties of a solid system are often determined by the presence of a liquid. This circumstance is especially true in systems composed of discrete particles, not only due to the high surface-to-volume ratio but also because the presence of a liquid dramatically affects the interparticle action −to a large extent through capillary forces. No matter the particles size, the influence of a liquid (above all, water [23]) in such *particulate systems* essentially relies on interfacial features at the nanoscale, which govern the behavior at the particle level. For instance, familiar examples are sand, which becomes 'workable' when is wetted by liquid films 5-nm thick or less on the grains [24], and flour in everyone's kitchen, which is sticky on rainy days through adsorption of a few water layers [25]. Set plasters are formed by gypsum crystallites linked by physisorbed water films ~ 1 to 10-nm thick (from dry to saturation conditions) [26]; similarly, clay swelling is typically due to moisture uptake of one to three water layers in the clay interlayer [27]. Friction and wear in soils, along with aging effects, depend on the presence of molecularly thin water films at the nanocontacts between mineral particles [28].

Particulate (or divided) systems generally refer to disperse phase systems containing particles disseminated in a continuous phase, and may extent, in the broadest sense, from protein solutions and bacterial cultures to interstellar systems [29]. In this article, we restrictively consider ternary solid-liquid-gas systems composed of a dense assembly of solid particles distributed in a gaseous environment that is partially filled by a liquid phase. These are referred to as (partially) *wet* or *unsaturated* particulate media, in which the liquid creates *pendular* (surrounded by gas phase) *bridges* between the particles exerting capillary interactions. By extension, one can include into this type *capillary suspensions* [30,31], which are dense particles-liquid-liquid systems governed by capillary forces. Unsaturated particulate media include solid colloidal aggregates [32], powders [33,34] and granular materials [35–,36,37]. Such systems are ubiquitous in nature (from soot to feathers to rocks and soils) as well as in technological and industrial materials, in intermediate or final form (coatings, desiccants, cements, pharmaceuticals, foodstuffs, modern ceramics, thermal and radiation shields, metallurgy...). Although the continuous phase in these media is formed, in principle, only by a gas (air, mostly), it virtually always involves some amount of liquid, frequently due to the mere adsorption of water from the moist surrounding. For example, the important influence of humidity in the mechanical behavior of powders and granular media exposed to habitual atmospheric conditions [e.g.–,38,39,40,41] shows that water must be almost universally considered. Thus knowing its interaction with particles is essential for e.g. materials science, biomedicine, civil engineering, mining, catalysis, oil recovery, agriculture and transport in soils, or even to prevent

erosion and natural hazards like landslides and avalanches.

Hence, the vast majority of divided media are wet particulate materials with huge practical interest. Nevertheless, most work has focused on dry particulate systems (solid-gas) [37,42,43] and, more recently, colloidal and granular suspensions (solid-liquid) [44,45] because of the much simpler binary-phase scenario −even so, they are still poorly understood. The additional fluid phase in the unsaturated case strongly complicates the picture and justifies that, apart from the phenomenology, the physics of wet particulate systems have been little studied and remains largely unknown [35,46]. One reason is that, although liquid-particles behavior relies on nanoscale phenomena, most research has been limited to relatively large scales, from millimeter down to micrometer (as in wet granular media [24,35,36,39,47]).Thus, new experimental and theoretical approaches are needed to facilitate access to smaller scales, which is especially challenging for bulk features in such opaque systems. Another reason is that the treatment of particulate media is fundamentally complex because they are composed of unequal particles with irregular arrangement. In the presence of a liquid, knowing the distribution and interplay of the different phases becomes an extremely difficult task, principally at the nanoscale. In order to overcome these difficulties, one can consider a kind of both 'tractable' and 'small' divided systems such as solid *colloidal crystals* (CCs), which commonly designates three-dimensionally ordered arrangements of self-assembled submicron, monodisperse spheres surrounded by air [48]. Thereby, in spite of the small particle scale, Brownian motion is suppressed by the compactness of the structure. Since the position, size and shape of the spheres are known, CCs constitute an attractive approach for the study of general features of particulate media.

Our laboratory has lately dedicated much work to investigate the interfacial water in CCs, which is taken up from the surrounding moisture in significant and controllable amounts. In particular, studies focused on silica CCs, being silica-water a most essential system in nature and technology. Among versatility and availability, CCs possess two prominent advantages: 1) they have a well-defined particles arrangement, as already mentioned; 2) as periodic dielectric structures, they exhibit *photonic bandgaps* (Figure 1) that, as it turns out, can be employed as a signal to probe water. Based on these characteristics, innovative methods have recently been developed to study how water is nanoconfined in the opal interstices [49]. In this article we summarize these latest techniques and describe former and new findings that not only teach about detailed nanometric features of water in opals but also open interesting perspectives on general, interdisciplinary liquid-solid physics. More specifically, we discuss possible links between CCs, as well-defined wet particulate materials, and general ternary particles-liquid-gas systems which are relevant in many different fields. Important aspects found in CCs, especially those dependent on water content, like mechanical properties, are pointed out as useful analogies to e.g. wet granular materials to be exploited in the future.

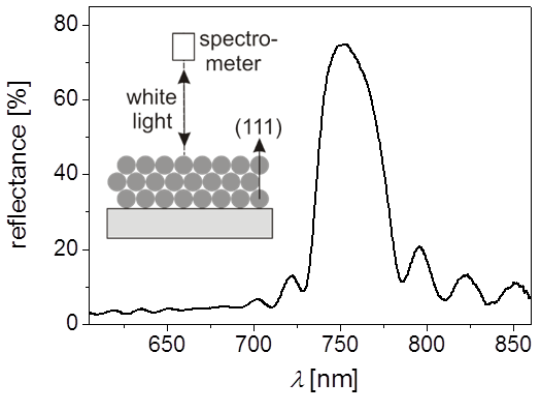

Figure 1 Typical reflectance spectrum of a CC (silica spheres with 335 nm diameter) showing a photonic bandgap (Bragg peak). Inset: sketch of the CC and the simple recording scheme.

2. Water in Colloidal Crystals

CCs (also referred to as *artificial opals*) are in their own right a relevant material class for numerous applications in photonics and energy [50,51], detection [52,53] or as atomic/molecular models [54]. For such uses it is important to know how the unavoidable presence of liquid (e.g. from condensation of a surrounding gas atmosphere) affects their performance, although historically this issue has barely received attention. Other applications of CCs as membranes [55], nanostructured platforms [56,57] and templates [58,59] depend on flow and diffusion processes of liquids in nanoconfinements such as the opal interstices. Any advance in the comprehension of these features is also beneficial for fields such as colloidal assembly or capillary/evaporation-assisted lithography [60,61].

We will show that CCs inherently contain a non-negligible amount of water picked up from the ambient, especially if the constitutive spheres are hydrophilic, as it occurs in typical cases like silica opals. Water is demonstrated to significantly affect the photonic properties of the ensemble, a fact that renders the CC a suitable *lab-on-a-chip* to study the behavior of the confined liquid. This method, which provides an indirect means to know the water morphology within the CC, is complemented by quasi-direct visualization of the water structures. Special attention is given to discern, under different conditions, how water is distributed, whether located between the particles as capillary bridges (*necks* or *menisci*) or on the spheres surface as a *wetting film*. The distribution of the liquid phase between the solid particles is decisive for the behavior of CCs as well as any divided system, as it determines aspects such as the intergrain capillary attraction or the flow of liquid across the medium. Presently there is no satisfactory manner to predict or measure such distribution.

2.1. Water Adsorption in Silica CCs

Submicron silica spheres (in particular, amorphous silica prepared by Stöber synthesis [62]) are extensively used for easy fabrication of high-quality face-centered-cubic (fcc) artificial opals [63]. Silica exhibits high hy-

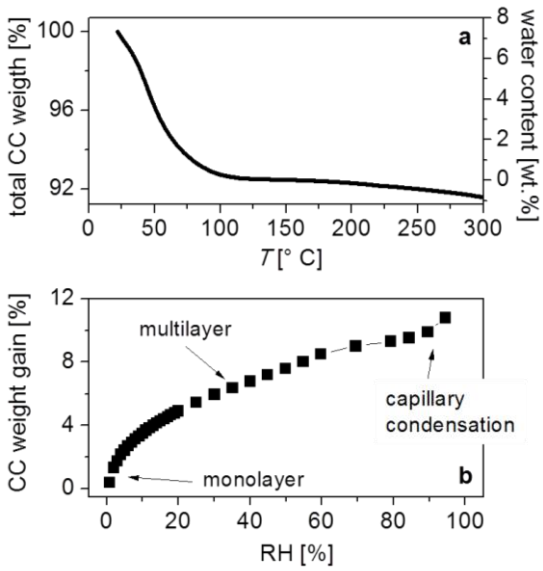

Figure 2 (a) TGA analysis of an as-grown silica CC (335-nm spheres). Adapted from Ref. 65 with permission. (b) Water adsorption isotherm on an as-grown silica CC (260-nm spheres). Adapted from Ref. 49 with permission.

drophilicity due to the presence of a large number of −OH groups (*silanols*) at its surface [64]. In a humid ambient, water molecules in vapor phase tend to adsorb on the silanol groups through hydrogen bonds, building a monolayer or, potentially, a multilayer of successively adsorbed water molecules, until a wetting film is formed on the silica surface. This type of water, loosely bound to the silica surface by physical bonding, is referred to as *physisorbed water*. Its content depends not only on the density of surface silanols but also on the ambient conditions, temperature (*T*) and relative humidity (RH), so this water readily begins to desorb (*desorption* or *dewetting*) by e.g. increasing the temperature or decreasing the ambient pressure. This amount of water in an untreated (*as-grown*) silica CC can be directly measured by thermogravimetry (TGA) from weight loss upon heating [65]. It is found that a very significant percentage of water, as large as ~ 7 wt.%, is physisorbed at room temperature (RT ≈ 25 ºC) and RH ≈ 40 %, which is easy to remove by gentle heating, until complete elimination at ~ 120 ºC (Figure 2a). Further heating leads to silanol condensation (at τ 150 ºC) and, consequently, loss of water affinity of the surface [65]. Such thermal annealing is a simple means to adjust the surface hydrophilicity of silica, which we employ to study the influence of the surface type.

The RH dependence of water uptake gives further insight into its provenience. Therefore, we performed water adsorption isotherms in the silica CC, confirming the large amount of water present (Figure 2b). The water content at RH ≈ 40 % approaches 7 wt.%, in accordance with TGA. The form of the isotherm is signature of initial adsorption of a monolayer of water molecules at low RH, followed by a remarkable multilayer formation [2]. The convex shape at RH < 10 % (isotherm type II) denotes the presence of narrow micropores (< 1 nm) in the spheres. Such pores are expected in Stöber particles [66] while larger micropores (1-2 nm) are discarded by nitrogen adsorption measurements [65]. Thus, further water adsorption (up to 90% RH) appears to be due to multilayer formation on the outer surface of the spheres, constituting the largest water contribution. Above 90% RH additional water uptake is visible, due to *capillary condensation* of water vapor in the porous CC structure, that is, in the gaps between spheres.

For sake of comparison, similarly large amount of physisorbed water and analogous temperature behavior have been reported in comparable silica spheres assemblies [63,66–68]. Water isotherms in cellulose and pharmaceutical powders also show a water content of ~ 6–10 wt.% at moderate humidities, largely due to multilayers [69]. Clay minerals show multilayer adsorption above 15% RH and contents of 5–10 wt.% at 40% RH [70,71], and setup of capillary condensation at 80% RH [71]. Capillary condensation is settled by the radius r_k of the liquid meniscus to be formed (Kelvin radius) given by $r_k = -\gamma V_m/R_g T \ln(\mathrm{RH}/100)$, where γ is the liquid-gas surface tension, V_m is the molar volume of the liquid and R_g is the molar gas constant. In the CC interstices, which are in the range of tens of nm, capillary water condensation sets in only at high humidities, when r_k is comparable to the pores dimensions ($r_k \approx 5$ nm at 90% RH). Capillary condensation at lower humidities would denote the existence of mesostructure. This is the case, for instance, of assemblies of mesoporous silica spheres with diameter in the 100-nm range, in which stepwise capillary condensation first occurs at 40–60% RH in the spheres pores of 2–6 nm, and later at ~ 90% RH in the gaps between spheres [52,72]. Such step at intermediate RH is absent in the CC.

Thus, silica CCs are macroporous structures naturally containing a considerable amount of water, mainly originated by multilayer adsorption in the voids formed between the spheres. It is worth noting that, before any measurement, samples were heated at ~ 120 ºC (for complete dehydration while keeping the silica surface unchanged) and cooled down to RT. Hence, spurious contributions like excess water in suspension [28,64] or remnants from opal fabrication [73] can be safely neglected. That is, we deal with water that truly comes from surrounding moisture and is an intrinsic part of the CC, along with the spheres and the interstices between them. In hydrophilic CCs like silica ones, the presence of water is very significant (7 wt.% water fills about half the volume of the voids of an ideal fcc opal), so it must surely be considered in order to faithfully characterize the opal. The distribution and behavior of this water in a CC was unknown until recently. Two original approaches were used to investigate the water morphology in such nanoconfinments, as described in the next Subsections.

2.2. PBG Method: The CC as Lab-on-a-Chip

A prominent use of CCs is as 3D photonic crystals. Indeed, the well-ordered spheres arrangement composes a periodic dielectric material, in which light cannot be transmitted in certain energy ranges, referred to as stop-bands or photonic bandgaps (PBGs). The lowest-energy PBG, or *Bragg peak*, is associated to the diffraction produced by the (111) family of crystallographic planes (Figure 1). The Bragg peak properties, described by the

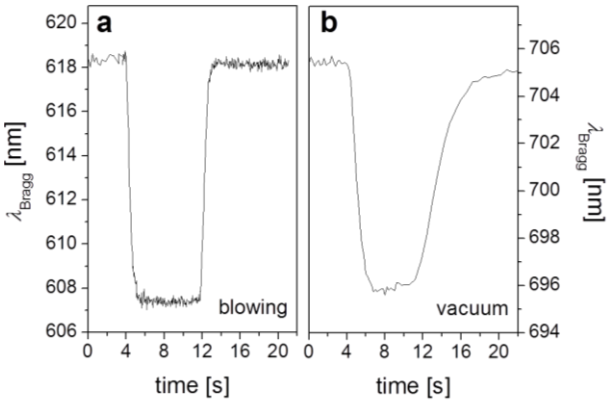

Figure 3 Bragg peak position (λ_{Bragg}) of different silica CCs during changing ambient conditions. (a) Dry air is blown against the sample (identical results were obtained using nitrogen). (b) Decrease of atmospheric pressure (low vacuum). The external action was set on and off at t=4 and 11 s, respectively. Note that the different time response are rather due to the dissimilar onset/offset times of the external action. λ_{Bragg} was calculated from in situ fast-recorded (intervals of 2 ms) spectra. Reprinted from Ref. 49 with permission.

position (λ_{Bragg}) and width, are determined by the CC parameters. On the one hand, the dimensions and packing of the spheres define the *lattice parameter a* (the side of the fcc unit cell) and the filling fraction of the spheres *f*. On the other hand, the materials building the opal give the respective refractive indices, that is, the spheres (n_s) and the media filling the voids (n_v). An intuitive but only approximated description of the Bragg peak position is given by the Bragg's law, which can be expressed (at normal incidence) as:

$$\lambda_{Bragg} = \left(4/\sqrt{3}\right) a \sqrt{f\, n_s^{\,2} + (1-f)\, n_v^{\,2}}\,. \qquad (1)$$

Although not described by the Bragg's law, the peak width depends on the dielectric contrast n_s/n_v and the lattice parameter, so that the width broadens for higher contrast and *a*. Experimentally, the width is taken as the full-width at half-maximum of the Bragg peak.

For an ideal fcc structure, $f = 0.74$ and $a = \sqrt{2}\, D$ (*D* being the spheres diameter). Conventionally, voids have been considered to be filled just by air ($n_v = 1$). However, the non-negligible fraction of water in the CC must directly affect its photonic properties. This fact is illustrated by two simple, qualitative experiments: 1) some gas (dry air or nitrogen) is blown against the silica opal; 2) the atmospheric pressure surrounding the CC is reduced. In both cases, the optical spectrum is simultaneously measured. Figure 3 demonstrates that λ_{Bragg} (and the width −not shown), significantly decreases in both tests, and it occurs in a reversible and fast manner. Such behavior has a trivial explanation if one considers the large amount of physisorbed water in the CC, which is susceptible to easily change upon variation of the ambient conditions. Concretely, in both experiments the water content decreases, and so it does the average refractive index in the opal voids, leading to blueshift of the Bragg peak (as simply deduced from Eq. (1)). The fast recovery of the shift demonstrates a rapid water re-adsorption by the CC. Such important role of adsorbed water, however, has been generally ignored and only exceptionally (and rather qualitatively) considered [63].

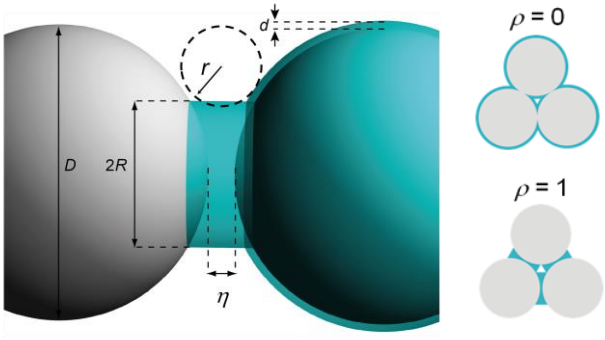

Figure 4 Left: Sketch of the modeled distribution pattern of the water in the CC assumed for the PBG method. A wetting film of thickness *d* on the spheres and a capillary neck between each two neighboring spheres, described by *R* and η, are distinguished. The meniscus radius *r* can be obtained geometrically. Right: Limit cases for the ratio ρ, for which water is uniformly distributed on the spheres as a wetting film (ρ = 0, top) or entirely accumulates in the necks (ρ = 1, bottom).

To establish a quantitative correspondence between Bragg peak and water is, however, more complicated because the PBG properties do not only depend on the amount of water. Indeed, its precise spatial distribution in the CC interstices is not included explicitly in the oversimplistic Bragg's law and only averaged in n_v and *f* values but decisively affects both peak position and width. The latter, which is often disregarded in opals characterization, is a pivotal experimental parameter to discern the water distribution, as discussed below. By adequately correlating the Bragg peak properties with a complete description of the CC (solid, liquid and gas phases), one can infer the morphology of the adsorbed water just by simple reflectance measurements. This is the approach we developed recently [74,75], in which the PBG is taken as a sensitive probe signal. Thus, the CC becomes a lab-on-a-chip, whose optical response provides access to structural information of any material within the pores network. We refer to this technique as the *PBG method*.

The procedure consists in correlating the measured Bragg peak with the exact water distribution by using a simple model (Figure 4, left). Hereby, it is distinguished between (1) water placed in the voids, which is assumed to build up a homogeneous wetting film with uniform thickness *d* around the spheres surface, and (2) water placed between nearest−neighbor spheres forming a pendular neck defined by size *R* (azimuthal radius) and thickness η (see figure). This bridge is assumed as axially-symmetric (gravity force negligibly affects capillary water in sub-millimeter pores [76]). Although such a liquid neck is known to generally approach a toroidal profile (*circular approximation* for capillary bridges [7,77]), the interface with air is here assumed to be flat for simplicity. The curvature of this interface (the meridional radius of the meniscus, *r*), which is relevant for the resulting capillary force (see Section 3.3.1), can be straightforwardly obtained geometrically by imposing the circular approach. The model considers $\eta \geq 0$, so some separation is allowed to exist between the spheres; that is, a nonclose-packed fcc structure is permitted for the CC. This is an important assumption in our model, as discussed later. Given the importance of capillary force,

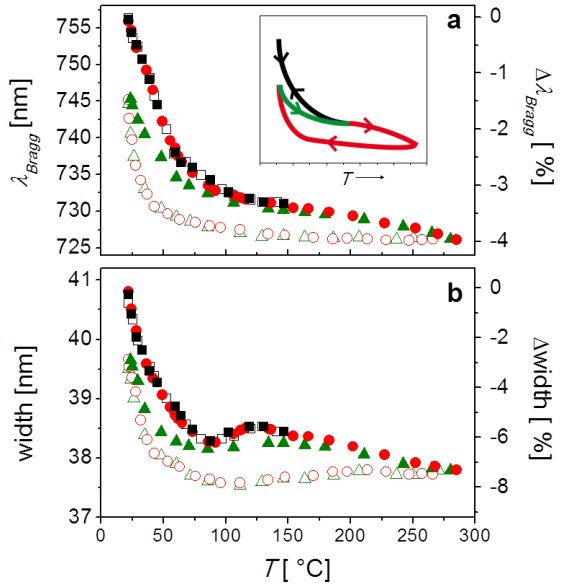

Figure 5 Evolution of the Bragg peak properties of an as-grown CC (335-nm silica spheres), λ_{Bragg} (a) and width (b) upon three heating/cooling cycles (solid/empty symbols with same shape each). Between RT and 150 °C (black squares and red solid circles), changes are reversible without hysteresis. After heating above 150 ºC (red circles and green triangles), partial irreversibility and pronounced hysteresis is observed. This behavior is schematized in the inset: below 150 ºC, black line; above 150 ºC, red and green lines. Reprinted from Ref. 74 with permission.

another relevant aspect is how much water accumulates in the necks. This fact is conveniently apprehended by a further parameter ρ, dependent of the other ones, which is defined as the ratio of the water bridge volume to the total water volume. Thus, $\rho \rightarrow 0$ when the water entirely forms a wetting film (no bridges), and $\rho \rightarrow 1$ when it builds only bridges between the spheres without wetting film (Figure 4, right).

The PBG method is applied to an experimental series in which controlled desorption of the physisorbed of CC is induced by gentle heating until complete dewetting, while measuring in situ the changes in the Bragg peak [74,75]. For each T, a number of triads of parameters {d, R, η} is compatible with the corresponding amount of water (known from TGA), so any triad describes a possible distribution pattern. Using a simulation software that calculates the exact solutions for the PBGs, the Bragg peak properties are obtained for each possible case. We performed accurate calculations based on the plane-wave expansion method, which allowed for the computation of heterogeneous periodic structures having a nonuniform distribution [74]. Finally, an iterative process finds the three variables {d, R, η} that fit best the measured PBG, and thus the water pattern in the CC is obtained along the experiment. Note that precise knowledge of the spheres diameter D is critical for the calculations (affecting the lattice parameter), but even electron microscopy yields a typical error of several nanometers, apart from the inevitable (although small) size dispersion. Measuring at the completely dewetted CC (T ~ 120 ºC) enables to accurately establish D (at least, an 'effective diameter'), as long as a strictly close-packed fcc structure is assumed when dehydrated.

Water desorption has a straightforward effect (typically, in about 1 s) on the Bragg peak properties (Figure 5), which basically resembles the progression of the amount of water measured by TGA (Figure 2a), confirming their close correlation. As long as the CC was heated below 150 ºC, the changes provoked in the PBG were fully reversible upon cooling the CC down and desorption and re-adsorption curves perfectly matched without hysteresis [74]. Such reversibility is a fundamental support that temperature only causes water desorption without any further structural changes in the opal, and it additionally confirms that we exclusively deal with water adsorbed from the ambient. By contrast, heating above 150 °C induced partial dehydroxylation of the silica surface [65] and prevented complete water re-adsorption, so the PBG did not fully recovered its original form and position at RT, showing a clear hysteresis loop.

The desorption data (up to 150 ºC in Figure 5) allow to obtain the parameters {d, R, η} in the hydrophilic (as-

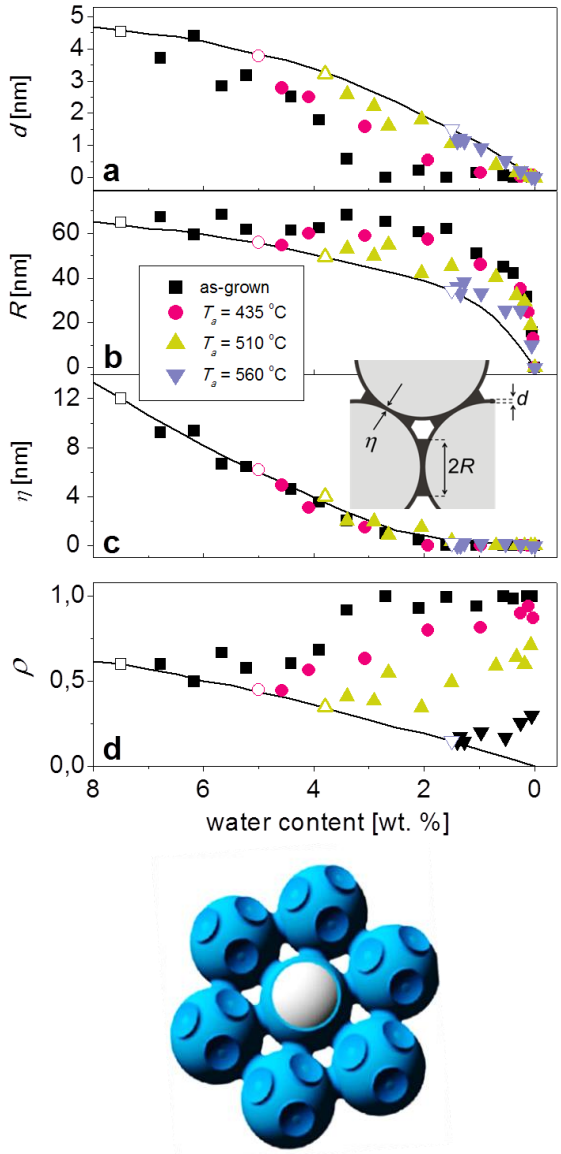

Figure 6 Top: Evolution of the parameters of the modeled water distribution (depicted in the inset) upon water desorption in as-grown (black symbols) and annealed (colored symbols) CCs of 335-nm silica spheres. Solid lines follow the values obtained at RT (open symbols). Bottom: Graphical representation of the water distribution (azimuthal view of an internal (111) plane) using the model parameters obtained for the as-grown silica CC at RT. Water in the central sphere is not depicted to remark the wetting film. Adapted from Ref. 75 with permission.

grown) silica CC between RT and complete dewetting. These are shown in Figure 6 (black symbols) as function of the water content (decreasing values to the right side of the figure, as it is the change direction in the experiment). At RT, the physisorbed water considerably concentrates between the spheres, building big necks (η = 12 nm and R = 64 nm; these values lead to $r \sim 20$ nm by assuming contact angle $\theta = 0^{\circ}$). The large η means that the spheres are substantially separated, forming a nonclose fcc packing. Note that this result is direct consequence of the pronounced narrowing of the PBG width upon desorption, until 6% reduction (Figure 5b). As the dielectric contrast increases (n_v decreases down to 1), the expected width broadening must be counterweighed by a marked reduction of the lattice parameter upon dewetting, which makes necessary a nonclose configuration at RT [74]. In spite of the accumulation in the necks (ρ = 0.6), water also builds relatively thick wetting film (d = 4.5 nm), which is consistent with the massive multilayer adsorption measured in Figure 2b. The modeled water distribution resulting from these parameters is graphically represented in Figure 6 (bottom).

Upon water desorption, two marked regimes are observed in Figure 6. First, down to ~ 2−3 wt.% water (T ~ 60−70 °C), both d and η quickly diminish until vanishing, while R keeps constant. At this point, all the remaining water is placed in the necks (ρ = 1), actually building an annulus around the contact points of the already touching spheres (close-packed fcc, η = 0). Second, below ~ 2 wt.% water (T τ 70º C), further dehydration leads to abrupt decrease of R, since the annuli are the last reservoir of water. On the one hand, this behavior shows that water on the spheres surface (more exposed without an adjacent sphere) desorbs more easily than the water between the spheres. This is in accordance with the general behavior in porous systems, in which higher temperatures are needed to dewet narrower pores, where the equilibrium vapor pressure is lower [1]. On the other hand, it seems that R remains constant until d vanishes, which suggests that water would flow from the wetting film, as long as it persists, compensating the volume loss of the neck.

The influence of the surface in the water pattern is studied by employing the PBG method on progressively hydrophobic (annealed at increasing temperatures) silica CCs (Figure 6, colored symbols) [75]. The gradual loss of hydrophilicity logically leads to less amount of water at RT. The {d, R, η} values deduced at the experiment start (empty symbols of each data set) show a well-defined trend (solid lines) toward 0 in a perfect hydrophobic CC. Note that the spheres tend to adopt a close-packed fcc arrangement in hydrophobic CCs ($\eta \rightarrow 0$). Simultaneously, ρ tends to 0, which indicates that the more hydrophobic the opal, the more uniform is the water distribution (the lower is the fraction of water forming bridges). Regarding the evolution of the parameters upon dewetting, two general conclusions can be drawn. First, each data set evolved nearly parallel to each other, indicating that, independently of the type of surface, water desorption proceeds almost identically as described above for the as-grown CCs. Second, none of the resulting water patterns coincides with one another, even at same water contents. In other words, the water always distributes differently on surfaces with different hydrophilicities, so the water pattern is unique for each type of surface. This finding eventually denotes that the surface energy affects the mechanisms determining the water distribution, which are discussed in Section 3.2.

These results show that a great deal of information on the behavior of nanoconfined water can be obtained by a simple optical procedure. The distribution of water in wetting films or necks between submicron particles and the influence of the surface hydrophilicity, which are most important subjects in nanoscale materials science, can be relatively easily studied and demonstrates the potential of the PBG method. Kinetics of water adsorption and bridge formation can also be studied in this way.

2.3 One-Pulse CVD: Imaging of Water Morphologies

Despite the described capabilities, the PBG method is an extrapolative technique which, in addition, takes account for the average behavior of the whole CC structure, so the verification of the deduced results by an independent means is desirable. Besides, the modeled distribution is expected to depart from the actual water morphology in some aspects like the homogeneity of the wetting film. An obvious goal would be to directly image the water in the particulate medium, which is actually a very difficult task, pursued in different systems since decades. For instance, in granular materials the gas-liquid phase has not been resolved below the micrometer range, even with exigent techniques like X-ray microtomography [78,79]. The use of optical microscopy requires the immersion in index-matching fluids [80,81], thus departing strongly from the original water-air configuration. Sophisticated techniques like environmental or in situ liquid-phase electron microscopies [82] allow direct submicron analysis but currently limited by factors such as restricted operating conditions or possible system distortion by the high applied voltage.

Scanning electron microscopy (SEM), as a customary facility in laboratories, would be ideal for inspection at the nanoscale but the required vacuum removes the water. However, a quasi-direct visualization of the water morphology would success if the water pattern is ‘fixed’ under ambient conditions previous to SEM inspection. We recently developed this approach in silica CCs by transforming the water into silica with a modified chemical vapor deposition (CVD) [83]. Standard CVD typically applies alternating pulses of $SiCl_4$ and water vapors for sequential silica growth and further wetting, respectively. In contrast, since we aimed to ‘catch’ only the native water in the CC avoiding any additional contribution, we used one single $SiCl_4$ cycle and no water pulses, so the reaction occurs only where moisture was previously adsorbed. Hence, this *one-pulse CVD*, performed at chosen ambient conditions, replicates the original water pattern into silica and allows submicrometric analysis by conventional SEM. Several tests, including simulations and experiments with variable pulse lengths, supported the reliability of the experiment [83]. It is worth noting that akin ‘fixing’ strategies have also been used in wet

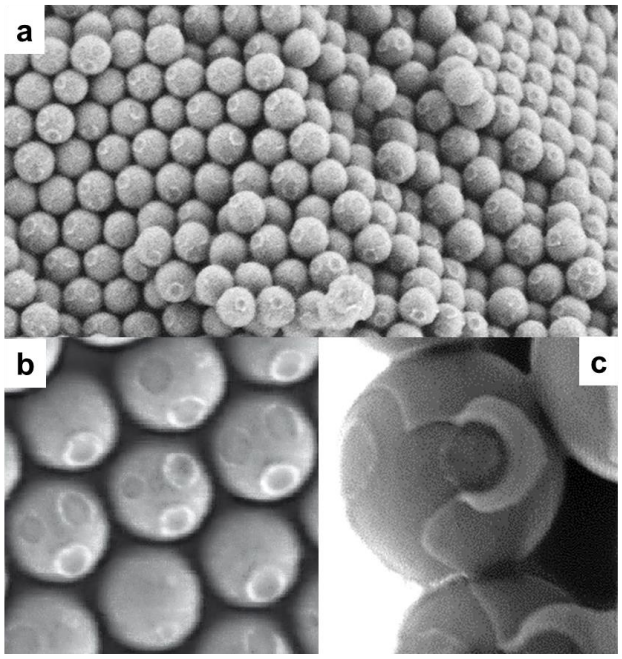

Figure 7 (a) SEM image of as-grown silica CCs subjected to one-pulse CVD at 25 ºC and 40% RH, in which the necks connected to the cleaved spheres are observable. (b) Azimuthal view of CC spheres. Missing necks denote arrangement imperfections. (c) Zoomed-in CC spheres, on which the wetting film is recognizable. Spheres diameter is 335 nm in (a) and (b), and 900 nm in (c). Adapted from Ref. 49 with permission.

particulate systems [31,80,84]. Thereby, a liquid polymer with low melting point serves as the wetting phase, which is solidified by lowering the temperature to allow electron microscopy imaging of the original morphologies. An obvious shortcoming of such approach is that it is only applicable with certain fluid phases, so the study conditions radically departs from the initial system. Concretely, if the polymer substitutes adsorbed water, essential original features can be missed.

The silica-transformed water structures in the CC resulting from the one-pulse CVD are indeed visible at SEM (Figure 7a). The patterns immediately confirm a main conclusion deduced by the PBG method: water predominantly accumulates between the spheres forming necks (Figure 7b), bearing a close resemblance to the graphical representation of the parameters in Figure 6 (bottom). The pendular state (non-connected capillary bridges) of the CC is also confirmed. This is significant because it indirectly supports two further results of the PBG method, namely the relatively thick wetting film and the nonclose spheres packing, although SEM images does not allow accurate estimate of d and η. Indeed, a large water amount such as 7 wt.% would otherwise lead to coalescent necks (funicular state) unless, first, a relevant portion resides on the spheres surface (ρ clearly less than 1) and, second, there exists some separation between spheres increasing the void volume. (In an ideal 335-nm spheres fcc packing, and without wetting film, the funicular state would occur up ~ 2 wt.% liquid). On larger spheres, a 'skin' coming from the transformed wetting film is observable (Figure 7c), which straightforwardly demonstrates that water can adsorb in stable nanometer-thick multilayers under standard conditions.

We also apply this technique using different ambient

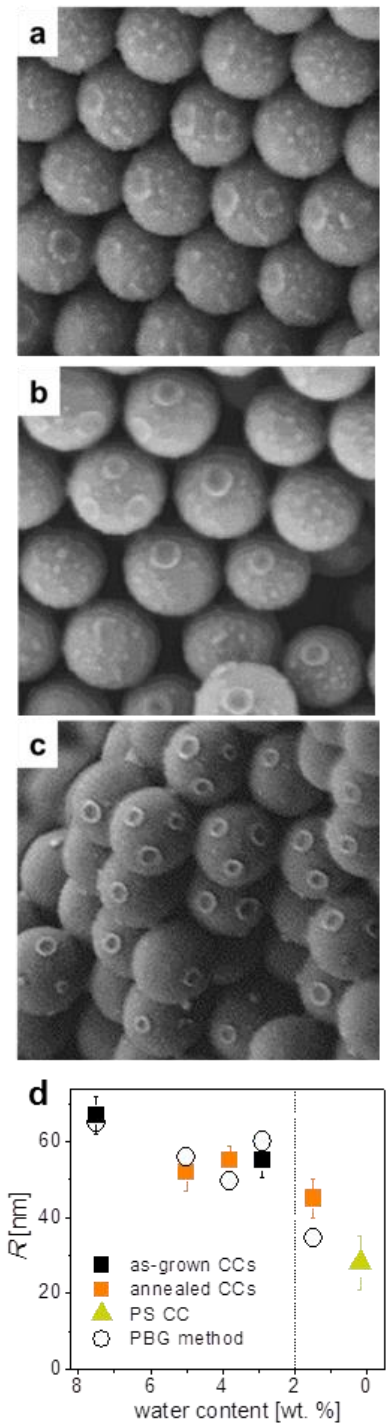

Figure 8 SEM images of different 335-nm spheres CCs subjected to one-pulse CVD at 40% RH. (a) As-grown silica CC, at 55 ºC. (b) 560 ºC annealed silica CC and (c) polystyrene (PS) CC, at 25 ºC. (d) Quantitative comparison, for different CCs and conditions as function of the amount of water, between the water neck radii R predicted by the PBG method (open symbols) and the (silica-transformed) values measured by SEM (solid symbols). The latter were calculated taking into account a reduction of ~ 25 % in volume due to transformation of water into silica [83]. Adapted from Ref. 49 with permission.

conditions or spheres surfaces. Figures 8a−c show some examples, in which the opals contain much less water (due to desorption or larger hydrophobicity). The images confirm another relevant feature predicted by the PBG method: the bridge size barely decreases upon significant reduction of the water content from about 7 wt.% (Figure 7b) to 3 and 1.5 wt.% (Figures 8a and 8b, respectively). Clear decrease of the neck size (Figure 8c) is only ob-

served at very low water contents, like in CCs made of highly hydrophobic polystyrene spheres (< 0.3 wt.% water at RT [83]). Even so, the neck size is still considerably large, which ratifies that water, when scarce, tends to wholly reside in the bridges between particles. In this case, d and η, although not measurable by SEM, must be vanishing small to allow such large R, as deduced in Figure 6. Together with the qualitative agreement, the predictions of the PBG method were also quantitatively endorsed, since a fair agreement with SEM values is obtained for the different situations (Figure 8d). The steep R decrease predicted in Figure 6b for water contents below ~ 2 wt.% (marked by the dashed line) makes this region much more sensitive (indeed, the accordance with SEM is worse) and, therefore, interesting for forthcoming studies.

Beside the strong support to the PBG method, visualizing the (silica-transformed) water structures also allowed the study of other aspects that cannot be concluded from the photonic properties of the CC. An interesting feature concerns the topography of the wetting film. While a quite uniform film is found on as-grown spheres under standard conditions (Figure 7), the scarce water remaining on them at higher T (55 ºC) or on annealed spheres rather builds nanodroplets (Figures 8a, b) [83]. This is a crucial aspect that tells us about the wetting and dewetting properties of a surface under different conditions and the arrangement of the adsorbed water molecules [85]. SEM images also allowed straightforward investigation of the effect of CC disorder in the water pattern, in particular, in the bridge size [83]. It was found that R diminished in the regions of imperfect spheres packing (a lower quality of the opal is easily stated by an inferior Bragg reflectance). In fact, R = 61 ± 11 nm, measured in less-ordered regions of an as-grown CC (reflectance below 50%), contrasted to R = 67 ± 5 nm in high-quality areas (reflectance above 75%). An increase of missing necks with disorder was also observed, although no quantification was made. Obviously, disorder of the fcc packing leads to larger average distance between spheres and less-regular packing, explaining the formation of less bridges, with smaller R value and higher dispersion. These features illustrate the influence of the particles packing in the bridge formation, which is a key aspect in particulate systems (see Section 3.3), for which this method easily provides quantitative information, even dealing with submicron water menisci.

As a last application example, the technique makes the silica-transformed capillary bridge readily accessible for direct analysis with nanometer resolution. The examination of small menisci has been so far elusive, although the precise knowledge their size and shape are critical (the more, the smaller the bridge) for calculation of the induced capillary forces (see Section 3.3.1). Furthermore, the bridge profile concerns the underlying Young-Laplace theory [86], whose validity may be questionable at small scales [87,88]. Figures 9a,b illustrates a fairly accurate description of the nanomeniscus formed between two silica spheres (in this case, they are not part of a CC). By taking the resulting D, R and d, we calculate r = 65 nm according to the abovementioned circular approximation, which surpasses about two-fold the observed curvature radius. This fact should attract attention to the possible deviation of the neck shape from a toroid at such scales [89,90]. Another features are deduced from the images. A thick adsorbed wetting film around the spheres is discerned and its thickness is straightforwardly estimated. Such a thick water film is consistent with the visible skin in Figure 7c and the values of several nm predicted for d by the PBG method (Figure 6a). The large neck size leads to merging in the presence of a further neighboring sphere (Figure 9c). Interestingly, water does not flood the interstice between the spheres (which contradicts observations and predictions elsewhere [47,78,79,91]), which is a relevant aspect because menisci need of the gaseous phase to exert a capillary force between the spheres [33,36].

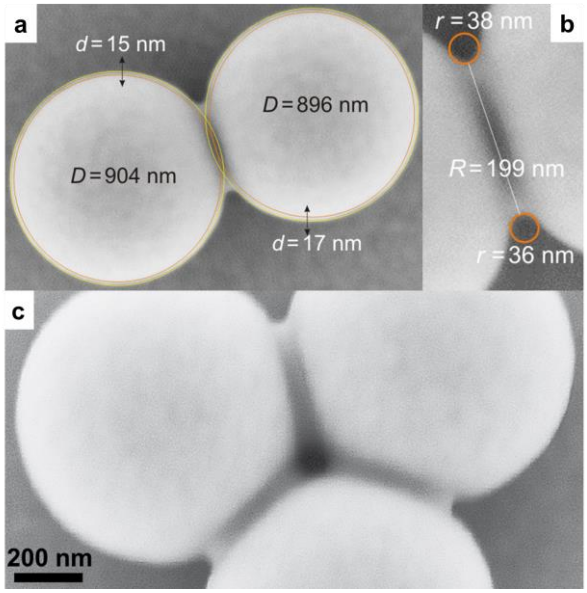

Figure 9 Geometrical analysis of nanomenisci formed between ~ 900-nm silica spheres. (a) Between two spheres; (b) Zoom-in of image a; (c) Between three spheres. Water was transformed into silica by one-pulse CVD at normal conditions prior to SEM imaging. Adapted from Ref. 49 with permission.

3. Colloidal Crystals and Liquid in Wet Particulate Systems: Perspectives

As seen, unprecedented quantitative information about the nanoconfinement of water in CCs has recently been gained from innovative optical and imaging means. The influence of factors like desorption or surface type has also been obtained. These data, when contrasted with macroscopic theories or measurements in planar systems, give insight into fundamental liquid-solid nanoscale topics and, further, singularities of not only opals but particulate systems in general. As an additional point of interest, since no water was added to the CCs, the results are particularly interesting regarding adsorption and capillary condensation in divided media.

In this Section we first discuss CC features like the massive multilayer adsorption and nonclose packing as they give clues to the interactions at particle surfaces connected by water. Second, the accumulation (or not) of water in bridges in the CCs is a notable aspect to look into. Indeed, the bridge formation is determined not only

by the energies at play in the system but also by the flowability of water at the nanoscale, the latter being intimately linked to the debated water structure and mobility in nm-thick films. And third, we examine the influence of water on the properties of the particles ensemble, whereby the most obviously aspect affected is its mechanical behavior. We analyze the cohesion of the CC and correlate with the individual water bridges and the forces exerted on the submicron spheres. We also inspect the rheology of CCs and identify analogies to granular materials. Along the Section, we point out nanoscale features found in the CC that are relevant in general particulate media and concern open questions to be addressed.

3.1. Surface Forces

Forces acting very close to a solid surface are responsible for the condensation of an adjoining vapor and critically affect the interfacial liquid [6], whose behavior may greatly differ from that in bulk. In turn, these forces are altered by the liquid. This interplay eventually determines two decisive characteristics: 1) the amount of adsorbed liquid; 2) the equilibrium distance between particles, which also defines the packing density. (In a particulate medium, the formation of capillary bridges and the subsequent interparticle adhesion result from these features −see following Sections). In CCs, these two characteristics actually lead to controversy: on the one hand, the massive water adsorption surpasses by far the expected value, and, on the other hand, the apparent noncontact between spheres denotes significant repulsive forces that need to be explained. These discrepancies reveal clues to the underlying surface forces in the CC, which are also present in every wet particulate system.

3.1.1. Wetting Film Thickness

The equilibrium thickness d of a film adsorbed on a surface is given by the *disjoining pressure* Π, which expresses the net repulsion between the solid-liquid and the liquid-vapor interfaces [86]. By considering only van der Waals forces, $d^3 = -A_H/6\pi\Pi$, where A_H is the Hamaker constant across the liquid film and $\Pi = -(R_gT/V_m)$ ln(RH/100). This predicts water film adsorption on a planar hydrophilic surface in air ($A_H \sim -10^{-20}$ J) of less than a monolayer for humidities below 80%. Nonetheless, water adsorption higher than expected has often been reported [6,92], including multilayer adsorption at ~ 50% RH of about 3 layers (d ~ 1 nm) [93,94] or even more (d ~ 1.5−2.5 nm) [95–97]. Such adsorption excess has been attempted to explain by adding terms to Π [6,92,93] although they cannot not fully explain the observations and their precise physical origin remains elusive. These contributions are principally electrostatic (*double-layer forces* due to surface ionization) or structural (*hydration forces* caused by ordering of the first water layers), while the presence of surface contaminants [92,98] must also be considered. In particular, the initial wetting of the silica can lead to surface ionization (and to subsequent electrical double layer) due to the silanol groups, which can also favor structuring of the adsorbed water layers [94]. Water film thickness drastically decreases on dehydroxylated silicas (Section 2.2 and literature [92,93]).

Contrary to the case of flat, open surfaces, the thickness of wetting films in divided systems is affected by factors such as the interfacial tension on the convex particles surface and the capillary pressure in the gaps at contacts [99], which additionally limit the wetting film thickness. In soil and plant science, for example, these different contributions are more usually accounted for by means of the *matric potential* Ψ, currently being an active research topic. Here we use it to estimate the maximum wetting film thickness predicted in a silica CC. In an ensemble of spherical grains of size D the impact of the interfacial curvature is included [100] to obtain $d^3 = -A/6\pi(\Psi - 4\gamma/D)$, where γ is the surface tension. By considering only van der Waals forces, $\Psi = -\Pi$ and $A = A_H$. At 40−50 % RH, $\Psi \approx -10^8$ Pa and d is practically identical to the value in planar systems, while hydration and electric double-layer would increase both Ψ (less negative) and d. However, from capillary scaling there exists an upper limit for the matric potential at which the bridges coalesce given by $\Psi = -9\gamma/D$ [100], and sets a maximum d that depends on the spheres size D. The large neck size measured above indicates that the CC is not far from this point. For 335-nm spheres, this limit is about -10^6 Pa, which yields d ~ 1 nm by taking $A = -10^{-20}$ J. Or and Tuller [101] find an "effective" A about six-fold the Hamaker constant, which would yield a maximum thickness close to 1.5 nm. In conclusion, adsorption of nm-thick wetting films in a system like the silica CC is theoretically feasible but the still superior thickness observed (d ~ 4 nm, that is, about 12 water layers) needs to be explained yet. A rigorous evaluation of the CC system using the concept of matric potential could be a convenient approach. Note that even thicker films were found on 900-nm spheres, which agrees with the trend of higher (less negative) limit to Ψ and, hence, larger d for larger D.

While the assessment of multilayer adsorption at moderate humidities is still debated in planar systems, the situation becomes even more complex in convoluted surfaces [3,102,103] like those in particulate media. Water film thickness may increase on corrugated surfaces in a manner not attributable to capillary condensation at the asperities. While roughness is known to affect the wettability of surfaces [5], it is less clear how it influences adsorption. In different systems, water adsorption appears to positively correlate with the material rugosity. For instance, adsorbed films on rough calcite were significantly thicker (2- to 40-fold) than those on smooth calcite [96,97]. Similarly, the thickness of brine films on silica increased over 100 times with surface roughness [104]. Multilayer adsorption is observed on rather hydrophobic self-assembled monolayers, from d ~ 2 nm at low humidity up to 4 nm at 65% RH [105,106]. Steps in mica terraces lead to nucleation of water deposits of height of 7 nm at 65% RH [107]. In the gap between a force microscope tip and a substrate, water condensation often surpasses the theoretical predictions, building e.g. structures of 15 nm height at 58% RH [4,108,109]. Results in soil science show that the adsorbed water films are significantly thicker in highly structured soils [110]. Indirectly, the abovementioned influence of moisture in

the mechanical properties of granular materials (sand, micrometer spheres packings) indicates formation of a significant number of capillary bridges, even at 10% RH [111], though the expected adsorption or capillary condensation cannot account for them. Indeed, increased vapor condensation arising from the proximity of neighboring surfaces and enhanced adsorbate–adsorbant interactions [2,3,99,112] must be considered, especially in submicron particles systems as their interstices approach the 1-nm scale. In view of these facts, the unexpectedly large adsorption found in CCs seems to be related to a more general phenomenon in divided media, and it remains an open question.

3.1.2. Equilibrium Interparticle Distance

Another controversial finding in silica CCs is that spheres are generally not in close contact to each other, showing a significant interparticle separation η up to 12 nm between 335-nm spheres, as inferred from the PBG method (Section 2.2). More direct evidence of such nonclose packing is desirable. Here we propose a simple approach, in which we make use of the ordered structure of a CC to determine its lattice parameter by fast Fourier transformation (FFT) from SEM images. The key is employing one-pulse CVD under the desired ambient conditions in order to 'freeze' the CC lattice, so it does not change under the SEM vacuum. Any spheres separation, in average, leads then to an increase of the lattice parameter when compared to that measured without water (in practice, by performing SEM without subjecting the opal to one-pulse CVD). We carry out the experiment on two as-grown silica opals, composed of 300-nm or 380-nm spheres, subjected to one-pulse CVD at 10 and ~ 40% RH. FFT is performed on areas of about 4 µm x 4 µm in order to average over an ample number of spheres while keeping high-quality arrangement (Figure 10a). Figure 10b shows a clear, progressive expansion of the CC lattices with increasing water content (higher RH), corresponding to growing η values (right axis). The resulting η at ~ 40% RH agrees well with that obtained from the PBG method for comparable spheres size (η = 12 nm), and strongly supports the "noncloseness" of CCs arrangements. Other techniques can be used to measure the lattice parameter vs. humidity for further verification, like atomic force microscope (AFM) −although the inherent difficulties linked to water condensation around the tip [113] must be considered.

The separation of the opal spheres leads to a filling fraction far below the close-packing value (f down to ~ 0.66 in the hydrophilic CC, much lower than the ideal 0.74). From the PBG method it was further deduced that η decreases with water desorption and in hydrophobic opals, reaching the ideal close-packed fcc (η = 0) below ~ 2 wt.% of water (Figure 6c) [75]. This behavior is consistent with the distinct filling fractions previously reported in fcc CCs, low in the case of hydrophilic spheres (f ~ 0.61) [67] and high with hydrophobic spheres (f ~ 0.70−0.74) [114,115]. Such differences can be now rationalized in terms of nonclose contact due to the presence of water, rather than disorder. In the case of much larger glass spheres (25 to 600 µm), a number of papers

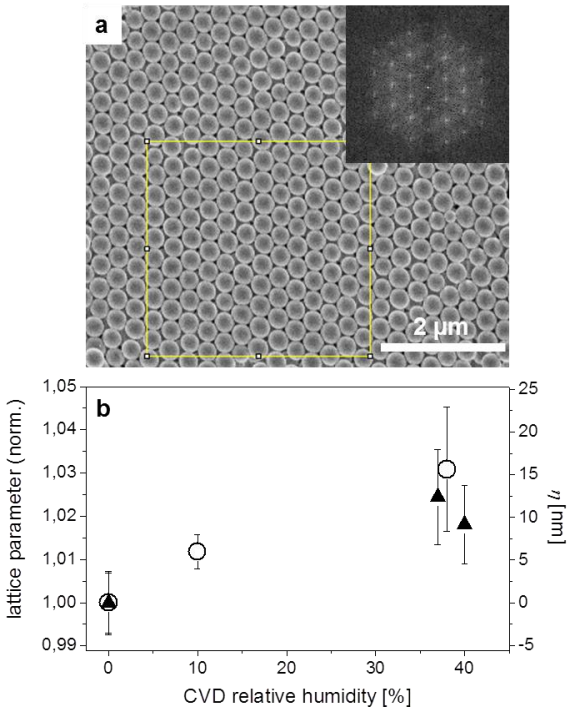

Figure 10 (a) Example of calculation of the CC lattice parameter on SEM images by FFT analysis (inset) of a well-ordered area (yellow square). The analysis typically extended over 10 to 20 such areas in each sample. The CC is previously subjected to one-pulse CVD at desired conditions (here, as-grown 300-nm silica CC at 38% RH). (b) Normalized lattice parameter (left axis) of as-grown 380-nm and 300-nm CCs (solid and empty symbols, respectively). Values at 0% RH were obtained by analysis of bare (not subjected to CVD) samples. The spheres separation η (right axis) was calculated for D = 380 nm (correction due to water-to-silica volume contraction was considered).

report wet (with added liquid) random granulates with f ~ 0.57−0.63 after compaction [79–81,116,117]. Pressed pellets of 75-µm glass ballotini showed f ~ 0.60 when wetted by water, and f ~ 0.63 by silicone oil [118]. These values are inferior to 0.64, expected in random close packings of monodisperse spheres [119] (actually, higher due to polydispersity: maximum f ~ 0.66 is measured in relatively dry 150-µm spheres [116]). Hence, apart from aspects like capillary adhesion or compaction dynamics [116], this fact could be indicative of finite separation between wet particles, especially with water.

The separation found between CC spheres points to the existence of significant repulsive forces between hydrophilic particles surfaces when (relatively abundant) water is present, which overcome the strong, attractive capillary forces. As the behavior of η shows, such repulsion seems to disappear with less water, or to be overcome by other forces. Coherently, as in the case for the nm-thick wetting film both hydration and electrostatic forces may also be accountable for surface repulsion and, consequently, equilibrium distances of several nanometers (note that the magnitude of η approaches 2d −Figure 6c). Mutual repulsion between hydrated solid surfaces like silica is long known and typically described by double-layer forces and, at small distances, also by the shorter-range hydration force [1]. Hydration repulsion has been found to dominate at separations of 1−5 nm in a number of systems [98,120,121]. Thus, hydration forces may justify the nonclose CC packing but, due to their

short range, would not explain such large η values, although hydration layers as thick as 7−8 nm have been reported in a suspension of colloidal silica spheres [122]. Probably, electrostatic repulsion has a main role, at least at longer distances. It is worth noting how the ionization of the wet silica surface and the large amount of water make the opal bear similarity to ordered colloidal suspensions. These are colloidal crystals formed in aqueous suspension (that is, a binary system), in which long-range double-layer forces, controlled by the ionization state of the system, lead to arbitrarily large equilibrium spheres separation [123]. In the opal, however, such an electrostatic contribution must be reconciled with the unitary behavior of η for all CC surfaces investigated (Figure 6c), which suggests no influence of the surface energy. Note that in hydrophobic CCs attractive *hydrophobic forces* can take place between surfaces [10], and would help reach close spheres contact. Finally, another factor to be considered is the mechanical behavior of water between the solid surfaces. Thin water films may exhibit high viscosity (as discussed in Section 3.2) and be difficult to be squeezed between surfaces, which would keep them at finite separation (viscous forces would diverge for vanishing distance) [124].

From this Section it should be concluded that meticulous evaluation is still needed to account for the role of surface forces and their water-dependence in CCs, a fact which is, in many aspects, common with general porous materials and particulate assemblies. Investigation of surface phenomena in these systems can benefit from comparing with the detailed experimental features achievable in the opal at the nanoscale, although being aware of the current limitations. The accuracy of the PBG method below a few nm is probably imperfect, and the resolution of imaging of the silica-transformed water structures must be enhanced in the future by using e.g. transmission electron microscopy or AFM. Even with the lower SEM resolution, the one-pulse CVD technique is useful regarding interfacial phenomena. For example, it makes available the study of the topography of the adsorbed films, in particular the occurrence of patches or clusters [83] (Figures 7 and 8), which determines the connectivity of the water phase. It also provides interesting hints regarding the particle contacts from the remaining bridges after detaching the silica CC spheres, on a hydrophilic glass substrate (Figure 11a) or between spheres (Figures 11b, c). The nonclose contact between the hydrophilic surfaces is now visually apparent from the bowl-like shape of the necks, with finite thickness in the center (Figure 11c). On the contrary, silica spheres leaves annulus-shaped necks on a hydrophobic silicon substrate (Figure 11d). Annuli are also observed between hydrophobic polystyrene spheres (Figure 8c; see Figure 13b also), which indicates close −at least, closer− contact when dealing with hydrophobic surfaces. The formation of annuli (with a wide central aperture) rather than necks with vanishing thickness at the center suggests the occurrence of an air meniscus (a bubble), instead of a water one, formed at the hydrophobic surface [125]. The set-up (*capillary evaporation*) and characteristics of such nanobubbles are enigmatic [126], and they have been long

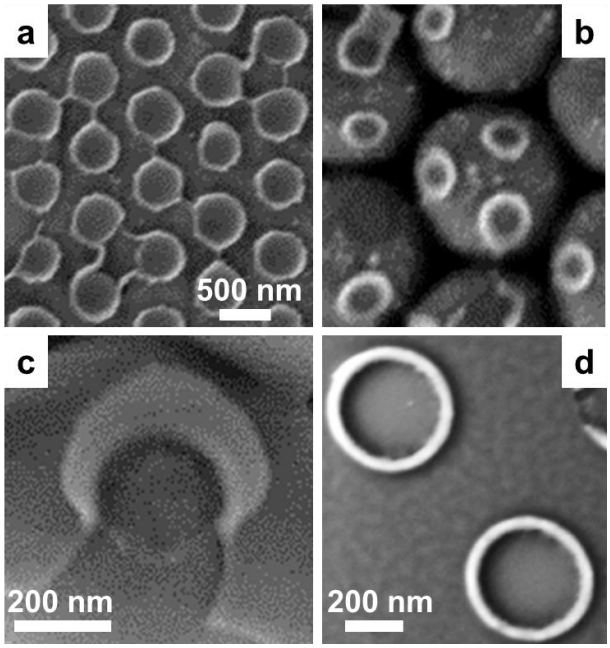

Figure 11 SEM images of (silica-transformed) water necks. Bowl-shaped menisci formed between 900-nm silica spheres (detached) and a glass substrate (a), and between 335-nm or 900-nm silica spheres (b, c). Annuli formed between 900-nm silica spheres (detached) and a hydrophobic silicon substrate (d). In all cases, one-pulse CVD was performed under standard laboratory conditions (25 ºC, 40% RH) prior to imaging. (a, b) are from Ref. 49, and (d) is adapted from Ref. 83 with permission.

proposed to elucidate the origin of long-range hydrophobic forces [125]. Hence, the simple one-pulse CVD technique would provide an easy approach to investigate this important surface science topic which remains incompletely resolved.

Beside the fundamental interest of surface forces and adsorption phenomena, they essentially affect the performance of any particulate system. The actual potential of the interfacial water determines not only the amount of condensed phase but also its distribution through the particles to form capillary bridges (Section 3.2). Liquid flow through the pore network is determined by the thickness and topology (connectivity) of the wetting film. These aspects are also critical for e.g. transport of colloids, radioactive waste, bacteria, etc. through unsaturated soils (vadose zone) [117,127,128] or (thermal, electrical, etc.) conductivities in packed beds for technological uses [57,129]. Particles separation strongly affects the capillary force exerted by menisci and its humidity-dependence [89,90] and, because the liquid fills the gaps, the intergrain friction or lubrication [130,131]. The equilibrium distance also defines the packing and porosity, which are key variables in complex transition phenomena in granular media like jamming and shear banding [42,132] and liquefaction [133], important in phenomena like landslides [134]. It can also lead to better understanding of swelling behavior of clays [27] and cellulose [38].

3.2. Capillary Bridges and Water Flow

In an unsaturated particulate medium, the distribution of the liquid phase on the surface of the particles (wetting film) and between them (bridges) greatly determines the interaction forces in the system. Specifically, the liq-

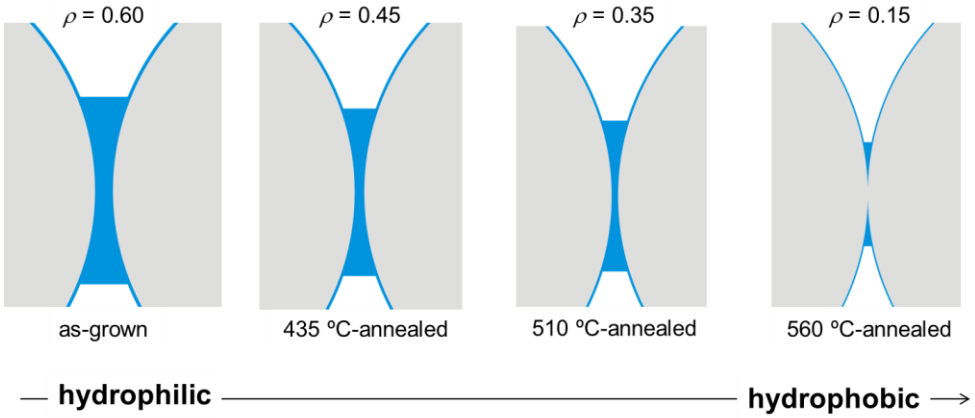

Figure 12 Water distribution (in blue) between two nearest neighbor CC spheres (off-cut side view) according to the parameters obtained at full hydration (open symbols in Figures 6a−c; drawn to scale). From left to right, progressively hydrophobic CCs are compared and the corresponding ratio ρ is given. According to the model simplifications, water necks are depicted with flat edges (instead of menisci). Adapted from Ref. 75 with permission.

uid bridges exert capillary forces between particles that typically surpass, in orders of magnitude, van der Waals attraction and electrostatic forces [33], and even gravity for particle sizes below 1 mm (large *Bond number*, which is the ratio of the capillary strength to the grain weight). Thus, capillary action dominates the interparticle adhesion and governs, together with viscous forces, the mechanical response of divided systems (Section 3.3), so the percentage of liquid accumulated in the bridges (the ratio ρ described in Section 2.2) is a prominent aspect to understand in such media. In turn, the resulting morphology of the liquid phase tells us about the nature of the confined liquid, its interplay with the solid surface and its ability to distribute within the particulate network.

One of the noticeable findings in the CC was the predominant accumulation of water around the spheres contacts to form large bridges, as described in Sections 2.2 and 2.3. Capillary condensation predicts, at thermodynamic equilibrium, a Kelvin radius r_k ~ 0.6 nm at the experimental conditions, which definitely cannot describe the observed menisci with radii r ~ 20 nm in 335-nm silica CCs (Section 2.2) or ~ 37 nm in 900-nm spheres (Figure 9b). Even considering surface effects, enhanced condensation would occur only very close to the contact between spheres and cannot account for the broad neck azimuthal radii (R ~ 65 nm in 335-nm spheres and, from Figure 9b, R ~ 200 nm in 900-nm beads). Actually, it is typically found that liquid concentrates at contacts, like between touching large-sized spheres [60,80,81,135]. Such large menisci are habitually assumed to be formed by *capillary suction* from the surrounding wetting film into the gap, as long as there exists enough liquid on the grain to allow flow [7,8,47,136]. In the case of the rough surfaces of large particles, this usually occurs only by addition of liquid or at high humidities. Otherwise, the liquid remains immobilized on the asperities and no bridges, or very small ones, are observed [80,81]. This argument has been claimed to explain adhesion experiments with micron spheres showing a threshold humidity, above which the meniscus is formed [137]. Viscous drainage from adjacent water films is proposed to contribute to slow formation of capillary bridges [138,139].

In moist submicron systems, this mechanism is less often contemplated [4], maybe because the precise distribution of liquid is rarely known or wetting films are expected to be negligibly thin. The allocation of water found in CCs suggests that capillary suction also works at such small scales. Herein, a minuscule water meniscus is first formed by capillary condensation at the spheres contacts or merging of the adsorbed films at the opposite surfaces. Due to the geometry, the meniscus is concave with negative Laplace pressure $\Delta P = \gamma(1/R - 1/r)$, the lower (more negative) the smaller the neck (smaller r) [4]. A pressure gradient with the neighboring water multilayers of the wetting film is then established, and water is drawn into the bridge to increase the Laplace pressure. (Note that this sequence is consistent with the behavior found upon desorption, for which it was proposed that water evaporation in the necks may be compensated by transfusion from the wetting film –Section 2.1). Water flow would be governed by the hydrodynamics laws and the final water distribution determined by the equilibrium between the Laplace pressure in the bridge and the disjoining pressure in the wetting film [7,8]. The latter is affected by the surface energy and influences the final water allocation, as seen in Section 2.2. In any case, this 'macroscopic' procedure assumes water fluidity in the nanometric wetting film, which is a questionable feature [19,140] as it concerns the mobility of water molecules adjacent to the surface, still being a matter of debate.

Indeed, numerous studies with a variety of techniques show that water transport is hindered close to a solid surface, the more the closer [e.g. 19,20]. In particular, viscosity increases or relaxation/diffusion times decrease in several (up to 10) orders of magnitude under confinements below d ~ 1-2 nm due to gradual structuring of molecules near different surfaces, including amorphous silica [130,131,141–143]. The first 3–4 adsorbed water layers (d ~ 1 nm) even may adopt ice-like [94,130] or chain-like [143] structures and motion is practically hindered. From capillary filling experiments, an immobile water layer of 0.9 nm has been estimated [4]. As we found in the hydrophilic CCs, the wetting film is thick enough (d ~ 4 nm in 335-nm spheres opals) to flow (at least, in the upper layers), although viscously. However, water transport is doubtful on hydrophobic CC spheres, on which d is much smaller. Besides, the topography of the wetting layer must also be considered, as the continuity of the film appears to fail in the hydrophobic case (Figure 8b), which would additionally hinder water

transport. According to these arguments, water can flow more easily on hydrophilic particles to accumulate in the bridges, while capillary suction would incompletely success on hydrophobic particles and necks remain small. These predictions perfectly agree with the behavior found in the CCs (Section 2.2): the parameter ρ, which describes the liquid concentration in the bridges (Figure 4), was large in the hydrophilic opals and progressively decreased in the more hydrophobic ones [75]. The water distributions obtained for the different surface types and same amount of water, which are drawn to scale in Figure 12, fully support the abovementioned statements.

In order to obtain additional evidence of the crucial role of the wetting film topography (and, eventually, of the surface nature) for water flow, we perform high-humidity measurements on different CCs. This way, sufficient liquid content on the spheres is ensured in order to rule out any transport inhibition due to a too thin wetting film. Figure 13a demonstrates the buildup of very large bridges between silica spheres, on which the wetting film is continuous. On the contrary, Figure 13b shows a polystyrene opal, in which a thick but clustered wetting film is visible on the spheres and only small necks were formed. Interestingly, the area surrounding the bridges perceptibly has less water. Note that the central zone between them, outside the 'suction area', shows again high droplets density. This strongly suggests that some capillary suction occurred indeed but strongly restricted to the closest neighborhood due to the non-uniformity of the wetting film.

Although quantitative analysis will be needed (examining e.g. to what extent Navier-Stokes equations are valid [13]), the way water distributes in a CC indicates that capillarity must be taken into account at the nanoscale similarly to micro- and macroscales. Capillary suction from surrounding wetting films (even being very thin) can help explain observations like the excessive water accumulation on AFM tips contacting a substrate [4,108,109]. It can also complement the explanation of a threshold in adhesion experiments between smooth surfaces [108,138,144], in which a minimum wetting film is claimed to be necessary for the formation of the capillary bridge. On the other hand, if suction is slow, it may contribute to sluggish growth of bridges [138,139,145], also leading to aging phenomena [30,39,146], which is often attributed to thermally activated capillary condensation [39,146]. Nanoscale topology and capillarity will have a great impact on imbibition and drainage in particulate media [147,148], fabrication and deterioration of building materials [149], water retention in soils [150] and water treatment [151]. Redistribution of liquid determines the number and size of capillary bridges in disperse media and eventually governs their mechanical properties, as discussed in the next Section.

3.3. Collective Behavior: Mechanical Properties

The most recognizable way in which a liquid affects the performance of particle aggregates is through their mechanical properties. Cohesion (stability against an applied stress) and rheology (deformation and flow behavior in response to the stress) are essential collective

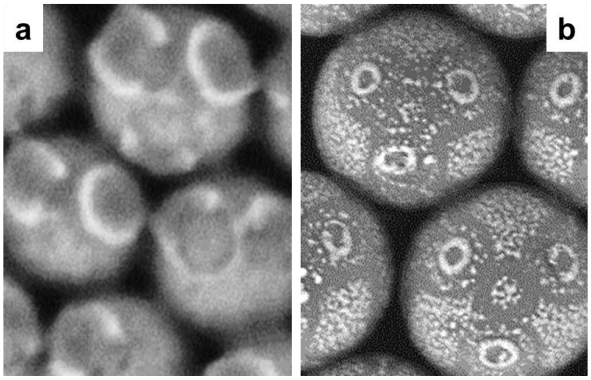

Figure 13 SEM images of capillary bridges formed under high RH atmosphere in CCs made of (a) 380-nm silica spheres, (b) 450-nm polystyrene spheres.

properties of a particle packing and critically depend on the intergrain adhesion, which is dominated by capillary forces in the wet case. Among the obvious importance of strength, deformability and flowability of wet particulate material [152], accurate comprehension of their cohesive properties is needed for many processes such as wet granulation and caking [38,69,153], fluidization [154], mixing and segregation [155], etc.

While dry particulate media are in principle cohesionless and purely frictional systems, the interstitial liquid in the wet counterpartners radically changes their mechanical behavior in two main ways. On the one hand, it leads to a cohesive ensemble through the capillary forces exerted by the liquid bridges between the particles, so the network structure is able to sustain a certain stress and mechanically behaves like a solid. Above a critical stress (*yield stress*), particles flow is initiated in the system, exhibiting a liquid-like behavior: a yield stress fluid. On the other hand, the interstitial liquid introduces a viscous force acting between the particles through the capillary bridge [33,124,156,157] that alters both the frictional behavior and the energy dissipation in the material, and introduces additional time-dependences in the system performance. While a dry granular material generally behaves as a viscoplastic medium [37] (flow properties depend on the deformation rate at sufficiently high rates), liquid may greatly enhance such viscous character. Among both capillary adhesion and viscous response at the contacts, other factors like slow meniscus formation or dissipative rupture and re-formation of bridges will also affect the rheological properties of a wet divided material.

It is well known that a minute quantity of wetting liquid drastically affects the cohesive properties of bulk powders, granular media and, lately, capillary suspensions. As mentioned at the beginning of this article, although most particulate systems contain some amount of liquid (often just from moisture), rather the limit cases have been preferentially investigated, i.e. systems with either empty or saturated pores. Actually, both dry granular media and dense suspensions, as binary systems, exhibit a parallel behavior and it seems to admit an unified description [158–160]. In contrast, such a framework is not applicable to wet unsaturated systems, in which the intricate liquid-gas phase generating capillary bridges

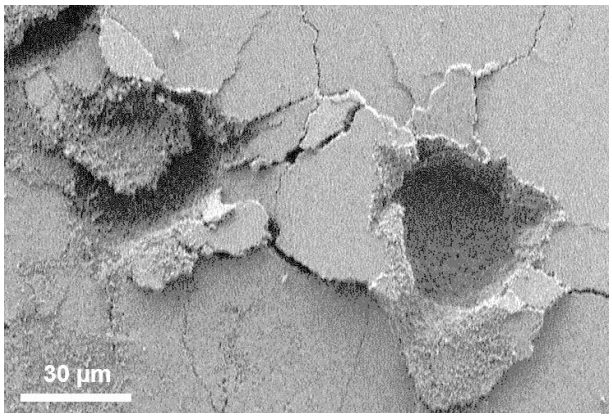

Figure 14 SEM image of a nanoindented silica CC. The mechanical deformation of the spheres assembly recalls common marks after digging in wet sand.

and their effect must be accounted for. This task becomes extraordinarily challenging because of the generally irregular arrangement, size, shape and roughness of the particles. Many of these difficulties are prevented in CCs, as discussed along the article, while the fundamental mechanical aspects remain basically the same. Indeed, in spite of the obvious difference in dimensions and arrangement, it is remarkable how indentations in a silica CC recall diggings in wet sand (Figure 14). Hence, a promising, and ambitious, perspective is to employ CCs as a mechanical analogue for fundamental investigation in granular science to allow simplified analysis of intricate features.

Only recently, comprehensive micromechanical characterization of *bare* CCs has been performed, for which nanoindentation was used [161,162]. Nanoindentation studies on *bonded* colloidal crystals [162,163] and assemblies [164] or nanoparticles agglomerates [165] missed most of the particulate features. A few other works have investigated colloidal ensembles by ultrafast optoacoustic [166] or microcompression techniques [167,168]. Nanoindentation procedure [161] consisted in indenting the opal by application of an increasing, at a fixed rate, loading force (P) while monitoring the penetration depth (h). At a certain depth of typically some hundreds of nm, *creep* (Δh) was measured at constant load during a dwell time, after which unloading is performed, showing how elastic/plastic was the deformation (Figure 15a). Hardness H and Young modulus E are calculated from the unloading behavior [161] to characterize the CC strength. Dependence on depth (Figure 15b) or loading rate (Section 3.3.2), and SEM imaging of the residual indents (Figure 15c) reveal structural and rheological aspects of the CC [161,162]. The loading curve readily reveals the granular nature of the CC by the occurrence of several *pop-in events* (Figure 15a, vertical arrows), which are caused by dislodging of individual spheres [162]. Temperature-dependent nanoindentation was further implemented to mechanically test silica opals with controlled amount of water [161].

Unavoidably, microscale characterization conceptually differs from macroscopic techniques used in granular media [37,170] to study yield stress (stability angle, compression, shear) and flow (inclined plane, shear), but

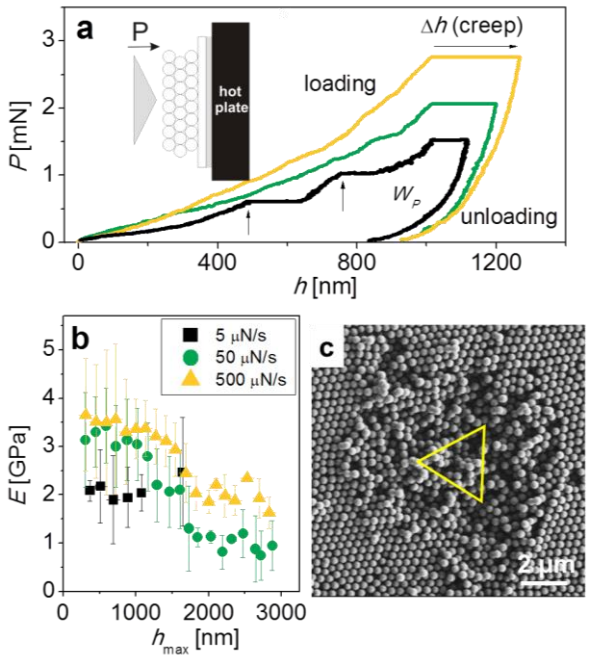

Figure 15 (a) Typical load–depth (P-h) measurements performed on a silica CC at three load rates (5, 50 and 500 µN/s –black, green, and orange lines, respectively). W_P is the plastic work (area between loading and unloading curves). Vertical arrows indicate pop-in events. Inset: scheme of the temperature-controlled nanoindentation setup. (b) Depth-dependence of indentation modulus E obtained at the different load rates. Values measured at h < 300nm are not considered because of significant indentation size effect [169]. (c) SEM micrograph of the residual imprint on the CC after indentation at h_{max} = 500 nm. The yellow triangle depicts the intersection area of the indenter (triaxial Berkovich type) with the surface plane at h_{max}. Adapted from Ref. 161 with permission.

it also depicts the cohesive and rheological properties of CCs. These are described in the next Subsections and parallelisms with the behavior of granular matter are discussed. A correlation between ensemble mechanical features and water bridge characteristics is here attempted.

3.3.1. Ensemble Cohesion

While extensive work has been made on capillary force at the grain level (exerted by an individual bridge between two surfaces), it has had less impact on the knowledge at collective level in ensembles. There, for a certain amount of liquid, the overall capillary force is determined principally by the number of formed bridges, which depend on the number of neighboring particles (up to ~ 6 in random close packings [119]) and the distance between them. A minimum amount is needed to, first, surpass the rough surface of grains, and, second, form a meniscus between non-touching neighbors, so the number of necks is critically affected at low liquid volumes. Thus, for increasing contents of wetting liquid, powders [171], granular materials [79–81,172,173] and capillary suspensions [30,31] show a rapid rise from vanishing yield stress to a stable value. This value corresponds to full pendular bridging (all particles contribute to the capillary network [31]) and remains constant along the pendular state, which indicates that further increase of the neck volume does not change the cohesion between the grains. Such independence is expected in macroscopic systems, for which the capillary force (F_{cap}) is identical for any liquid bridge, as long as the grain size D (assumed to be spherical) is much larger, i.e. $r \ll R \ll D/2$

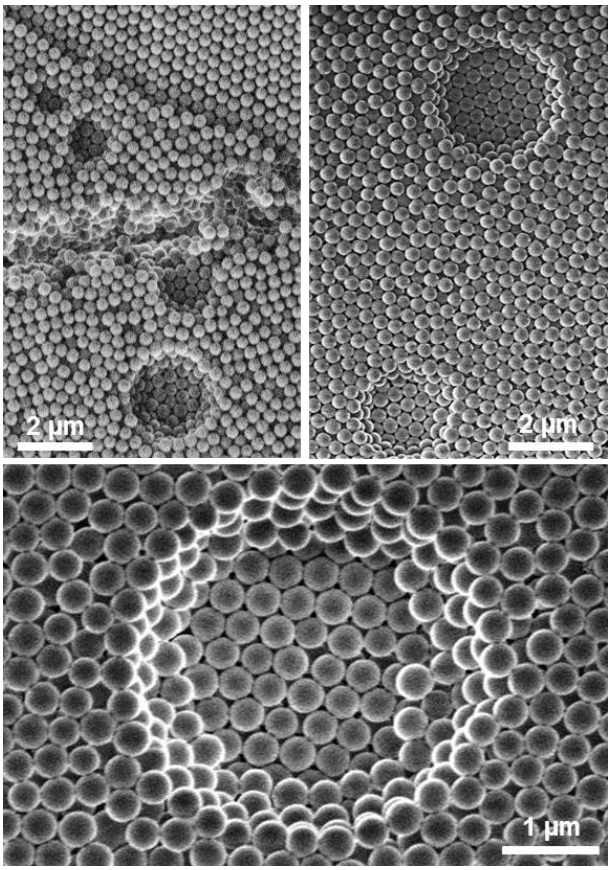

Figure 16 SEM images showing pronounced loss of spheres in disordered layers of silica CCs. No detachment of spheres is observed in the well-ordered layers.

(*standard approximation*) [1]. However, for growing liquid contents, the neck becomes comparably large and F_{cap} depends on its volume and shape (see below). In irregular packings, though, this fact overlaps with the beginning of bridge merging (funicular state), where the overall capillary force also depends on the liquid phase connectivity, as it determines the bridge interfaces [79]. These factors and the a priori unknown liquid distribution make quantitative information to be hardly accessible. Hence, the correlation between individual bridges and collective cohesion is missing in granular matter, especially in the relevant low water content regime.

In contrast, in fcc-packed CCs all bridges are equal, comparable in size to the spheres, and their number is readily known (every sphere is ideally connected to 12 neighbors, and namely by any amount of liquid). Being the fcc packing the most compact arrangement (with shortest interparticle distance, i.e. largest F_{cap} [7], and highest coordination number), the cohesion is expected to be maximal in a CC and any disorder should diminish it. This statement is illustratively proved in a particular silica opal exhibiting significant misarrangement in the upper layers (Figure 16). Flaws in the CC (due to e.g. air bubbles or cracks) leads to detachment of many spheres from the disordered layers, indicating poor cohesion, while no spheres are missing in the lower planes with well-ordered, highly stable arrangement. The decrease of the number of menisci was assessed by the one-pulse CVD technique, together with some reduction of the average neck size (Section 2.3). Strength measurements of the ordered CC [161] support these assessments. H and E values, respectively ~ 0.15 and 3 GPa at standard conditions (Figures 17a,b), comparable to those in similar systems [162], are in the range of hard polymers, demonstrating a remarkable robustness for a bare particulate ensemble. In wet granular random packings [173], E values calculated from elastic shear modulus were below by a factor of at least 5 −after correcting the dependence with the particle size−, which we attribute to the disorder. Depth-dependent experiments in the CC showed that E clearly decreased at deep indentations (Figure 15b), as the fcc packing was increasingly distorted (H exhibited a similar behavior in this CC [161] and others [162]). Such order effect in the system cohesion is also observed in polymer colloidal aggregates [163], in which E of semicrystalline zones was twice as large as that of amorphous regions, a factor close to that observed in Figure 15b.

In this sense, the CC shows a brittle behavior as the structure becomes much more compliant after a short deformation strain. Such performance is also found, for instance, in wet powders caused by high packing density and strong attractive forces [153], as it is the case of the opal. Reynolds dilatancy, which is the tendency of dense granular assemblies to expand upon strain because of steric exclusions, must be considered as it leads to larger interparticle distance and thus to decreased capillary forces in a wet particulate [172]. Another important feature for both granulate stability and transmission of deformation is the creation of a network of particles contacts in dense granular matter [174], which transfer the stress through the ensemble. Upon indentation, such *force chains* are created preferentially in the strain direction [172] and leads to distortion of particles layers far below the indenter [163,175]. This accounts for the drop of H and E measured in the CC after penetration of h ~ 1200 nm, i.e. about 4 spheres planes (Figure 15b), which would not be explainable only by disarrangement of the upper layers. SEM images of the residual indents (Figure 15c) corroborate that the distortion of the opal structure (in this case, on the film plane) clearly exceeds the indented area over several microns even upon shallow indentation. The reach of stress transmission is enhanced by the crystalline structure [163,176]. The imprint profile, although reminiscent of the triaxial shape of the employed indenter, is notably smeared, which emphasizes how slight packing irregularities (defects are small in the high-quality opal) lead to markedly asymmetrical force chains [176]. Upon deeper penetration, shear bands are observed [161,162]. All these aspects, decisive for the stability of any particulate material, has maximal impact in the CC because of its highest compactness and crystallinity, so their granular features may help analyze the dependences on packing density, contacts networks and, in addition, cohesive forces.

Temperature-dependent nanoindentation allowed to measure the CC strength upon dehydration [161]. Here, in order to emphasize the role of the capillary bridge, we plot the resulting H and E values as function of the desorbing (as it is the change direction in the experiment) water content (Figures 17a,b). We first notice that the experimental error was higher in the presence of water

than in its absence (T τ 120 ºC). We also found this trend in other works on water-controlled adsorption [135,144,177], which suggests high sensitivity of the resulting force to slightly dissimilar water necks along a single experimental series. The CC strength clearly reduced from 'wet' to 'dry' state about a factor of two. Similar factors are reported in numerous pull-off force experiments between relatively smooth surfaces [136–138,144,178]. This suggests that this remarkable 'dry adhesion' is due to van der Waals attraction, which increases when water desorption proceeds, because spheres surfaces approach close contact and the Hamaker constant is about ten times larger in air. Hence, the friction between sliding spheres is probably less significant. It must also be considered that vanishing amounts of strongly bonded water could persist at T τ 120 ºC and lead to non-negligible capillary adhesion [136,179]. In any case, the non-collapse of cohesion supports that basically all neighboring spheres are in close contact after dewetting, which is allowed by the well-ordered opal arrangement (H and E are measured at low penetration depths, so distortion of the bulk fcc packing is negligible). Thus, the number of necks (and, later, of dry contacts) can be considered approximately constant (equal to 12) along the whole experiment. It also indicates that spheres roughness, which would radically preclude meniscus formation at low water contents and reduce the dry contact surface [180], is not determining in the CC features. Both aspects, not fulfilled in powders or granular matter, are crucial to simplify quantitative analysis in studies performed on CCs.

The strength difference between wet and dry states evidences that the existence of capillary bridges clearly increases the opal cohesion. Within the wet range, H and E seem to diminish with decreasing water content before complete desorption but the trend is not sufficiently conclusive. Nevertheless, it can be assessed that the CC cohesion varies less pronouncedly than the amount of water. Correlation of the macroscopic cohesion of an ensemble with the interparticle forces has not satisfactorily been resolved to-date. The classical Rumpf model [33] simply describes the tensile strength σ of a disordered granular assembly as proportional to the interparticle bond strength F exerted by an individual bridge, assuming equal bridges and particles size D and known coordination number. These assumptions are generally unrealistic in particulate systems but true in a CC. For instance, by considering yielding along the (111) plane of an ideal fcc packing, the CC hardness is given by $H = 3\sigma = 18F/D^2$ [162]. Often, F is assumed to be mainly due to capillary force, as in assemblies with relatively large particles bound by low-viscous bridges [33]. However, the ensemble strength can be importantly augmented by dissipative contributions like interparticle friction and viscous forces [33,118].

Indeed, F ~ 900 nN is obtained for the CC from the experimental H ~ 150 MPa, which largely surpasses the value of F_{cap} ~ 60 nN for a single capillary bridge (see Eq. (2) below). This discrepancy is quantitatively less because, on the one hand, the expression of H, which is deduced from the tensile strength, may significantly

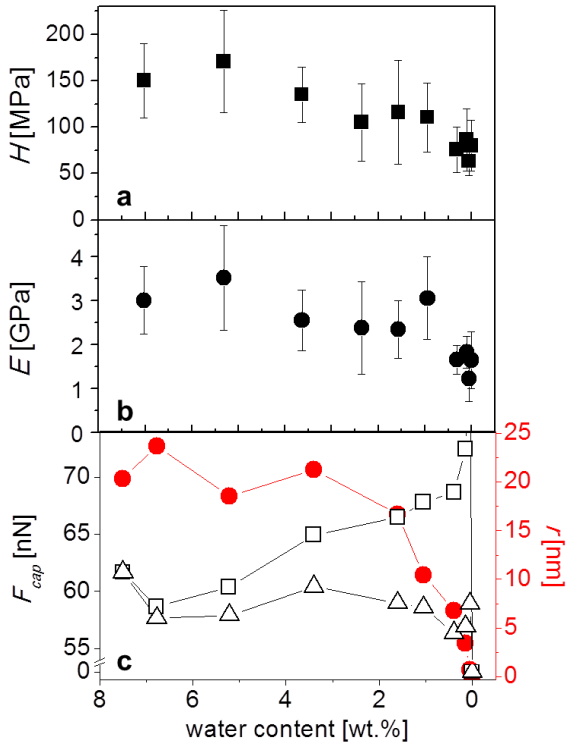

Figure 17 (a, b) Dependence of hardness H and modulus E of a silica CC with the water content, measured by temperature-controlled nanoindentation at h_{max} = 600 nm and rate 50 μN/s. (c) Left axis (open symbols): capillary force F_{cap} individually exerted by the water meniscus between two CC spheres, considering either constant or temperature-dependent surface tension γ (squares and triangles, respectively); right axis (solid circles): meniscus radius r as calculated from the bridge parameters (Figure 6) obtained from the PBG method. Data in (a, b) are taken from Ref. 161 and represented against water content as calculated from T in the original experiment and using TGA from Figure 2a.

overpredict F in a compressive experiment like nanoindentation [118], and also neglects the force chains [34], surely important in the CC. On the other hand, if the actual meniscus radius r were smaller than expected, as we already observed in 900-nm spheres (Figure 9), the calculated F_{cap} would increase (Eq. (2)). In any case, this estimate shows that the 'shear resistance' of each sphere contact against deformation of the CC in the wet range is largely due by friction and viscous forces, probably dominating over capillary interaction. In this sense, F would approach the *dynamic liquid bridge force*, which is the sum of capillary and viscous forces [156,157]. To evaluate how these mechanisms correlate with the characteristics of the bridge, whose viscosity is unknown, thickness-dependent and probably much higher than that of bulk water, is a challenging issue to be tackled in the future.

In spite of not knowing the weight of capillary forces in silica CCs cohesion, the precise information of the water necks we gathered gives an opportunity to evaluate the progress of F_{cap} exerted by an individual bridge upon desorption (Figure 17c), and juxtapose with the micromechanical strength. It eventually concerns how behaves F_{cap} between micro/nanometric surfaces, where D is too small to justify the standard approximation. A compact expression for a pendular bridge is given by [49,124]

$$F_{cap} = \pi\gamma R(1+R/r), \qquad (2)$$

which explicitly shows the dependence with the bridge size (through R) and curvature (through R and r. (Note that Eq. (2) slightly varies depending on which point of the bridge is considered to evaluate F_{cap} [33]). Empirical demonstration of these dependences is actually lacking in the literature because of the inaccessibility of the necks characteristics at small scales. Most studies, both experimental and theoretical, actually investigate F_{cap} as function of the relative humidity, where the bridge volume is unknown and must be assumed from theoretical adsorption and capillary condensation. Moreover, these standard approaches appear to fail in predicting the bridge morphology in a particulate system such as the CC, as discussed in Sections 3.1 and 3.2. Here, in contrast, F_{cap} between any two opal spheres is directly calculated from Eq. (2) and the known $\{d, R, \eta\}$ parameters (Figure 6). Unfortunately, since the meniscus radius r is not provided by the PBG method, the calculation is limited by the necessity of imposing a bridge profile, in our case, a toroidal interface (the abovementioned circular approximation). The resulting r (solid symbols in Figure 17c) decreases for smaller bridges, and consequently F_{cap} shows, by taking $\gamma = 0.072$ N/m, a general increase upon desorption until it drops to zero by no water at all (open squares). However, γ significantly decreases with temperature [179], which is important for heating experiments. By taking this fact into account, an overall but slight (about 10%) decrease of F_{cap} is obtained in the wet range, except at vanishing water contents when F_{cap} diverges (open triangles in Figure 17c). Note that same trends are also obtained using more sophisticated expressions for F_{cap} [7,181].

Most literature on experimental adhesion between small, individual surfaces shows decreasing F_{cap} with decreasing water volume, at least below a certain amount (in humidity experiments, below 30–60% RH) [108,136,138,144,177,178,182]. Disparate and system-specific behaviors have also been reported, sometimes explained by micro/nanoscopic features like surface roughness precluding meniscus formation at very low amounts of water [138,180,183], influence of the wetting film [181,184] or behavior of the confined water layers [88]. The counterintuitive increase of F_{cap} with shrinking bridge in Figure 17c (for constant γ) must be attributed to the circular approximation, according to which the decrease of r dominates over that of R^2 upon volume reduction (see Eq. (2)). The toroidal assumption also leads to a divergent F_{cap} for vanishing water contents, which should have been noticeable in CC cohesion; however, clearly lower values were measured below 0.5 wt.% (Figures 17a,b). As mentioned earlier, the capillary bridge contour probably deviates from a toroid at submicron scales. More importantly, the formulation employed derives from a continuum description of the liquid bridge, which must gradually fail under certain volume. In fact, calculations of the exact profile of nanomenisci lead to decreasing F_{cap} for decreasing bridge volume [88–90,185].

The analysis here performed exemplifies how the simplified features of opals allow progresses in understanding cohesion in particulate media, but it remains a complex task. Dissipative interparticle forces may importantly contribute to the strength of an ensemble, due to friction and, probably to a larger extent, viscous forces generated by the nm-thin capillary bridges between particles. Dissipation caused by rupture of bridges must also be considered. Quantitative description of capillary forces needs to be further improved, for which the meniscus curvature is a critical parameter. Direct access to bridge characteristics would be greatly helpful but difficult, especially at small scales, for which the one-pulse CVD, applicable to any system, emerges as a useful empirical tool for meticulous SEM examination. Finally, though system-specific, one should not forget water-assisted phenomena like softening, dissolution or corrosion that affect granulates cohesion through e.g. plastic deformation of grain asperities (larger contact area), crystallization of solid bridges or chemical change of the surface [28,167]. Some of these processes may contribute to aging in humid granular materials [39,186].

3.3.2. Rheology and Rate Dependence

Flow in powders, granular materials or suspensions is typically investigated by shear experiments [37,170]: the medium is sheared between two rough walls moving at a relative *shear rate* and the *shear stress* developed tangentially to the motion (i.e. the resistance to yielding) is measured. In contrast, information about rheology of CCs has been accessed so far only through nanoindentation [161], whereby the micromechanical performance is tested for varying rates of compressive loading. Regardless the experimental approach, the essential aspect of how the material response depends on the velocity of deformation is obtained, and, thus, the frictional or viscous behavior of the system is determined. In any case, contrary to dry granular media and suspensions, rheology and rate-dependent deformation in wet particulate systems [30,31,40,116,156,157,187,188] have been little investigated, so the CC offers a good opportunity to gain insight into them.

P–h curves (Figure 15a) readily demonstrate that the CC is more resilient to yielding (steeper loading curves) upon growing load rates and, correspondingly, H and E increases with the rate (Figure 15b). Such rate-dependent performance evidences a marked viscoplastic response [161] and is comparable to the behavior usually observed in dense suspensions [159,160] or capillary suspensions [31], in which the shear stress increases with the shear rate. Typically in nanoindentation experiments, the viscous character of a medium is revealed by the occurrence of creep displacement Δh (Figure 15a) [169]. Creep is consequence of the retarded reaction of the material, which remains flowing in response to the deformation energy stored in the structure during the loading; hence, the creep depends on how fast the stress has been induced. In a viscous medium, Δh is larger and evolves faster with increasing load rate. Measurements on opals [161] demonstrate, at ambient conditions, both large and remarkably rate-dependent Δh (black solid symbols in Figure 18a), and the creep dynamics clearly speeds up with the load rate (lines in Figure 18b). These facts straightforwardly endorse the viscous nature of yielding

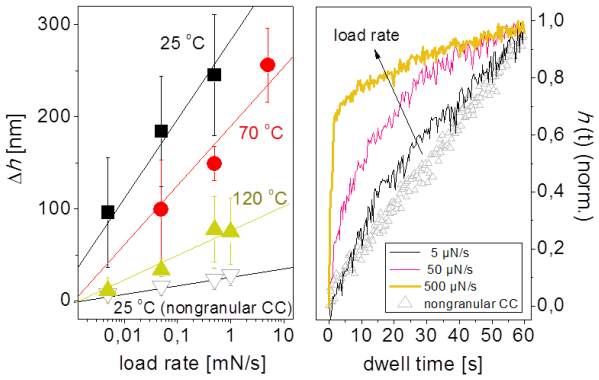

Figure 18 (a) Dependence of the creep displacement Δ*h* with the load rate measured by temperature-controlled nanoindentation (dwell time of 60 s) at load rate 50 μN/s on bare (solid symbols) and a CVD-infiltrated (empty symbols) silica CCs. Lines are linear fits. (b) Normalized transient creep *h*(t) measured at 25 ºC in bare silica CCs with increasing rates, and in the 'nongranular' CC (at 50 μN/s –no rate-dependence was observed). Adapted from Ref. 161 with permission.

in wet CCs. Moreover, temperature-controlled nanoindentation allowed to follow the creep behavior as function of the water content [161]. Indeed, Δ*h* and its rate dependence, manifestly decrease in heated, that is, drier CCs (Figure 18a). The remnant creep observed at $T \geq 120$ ºC (or 0 wt.% water) can be compared to the viscoplasticity exhibited by dense dry granular media at rates high enough [37].

Such behavior demonstrates the key role of water in the CC viscosity, though it remains to question how it causes the rate-dependent response. In granular materials, rate dependence may occur because of slow formation of capillary bridges, due to slow condensation with characteristic times of several minutes [39,40,111], or viscous transport of the liquid across the pores network [80,189] through ~ 100-nm-thick wetting films on micron-sized grains. However, in the experimental time scale, bridge evolution in the CC would not explain the viscous behavior. On the one hand, water adsorption in silica CCs is fast, with characteristic times of less than ~ 1 s (Section 2.2) or even milliseconds [190]. On the other hand, the high viscosity of water in the nanometer-thick wetting films would preclude significant macroscopical flow across the opal. In any case, slow bridge development causes the formation of less and smaller bridges (lower *Fcap*) during particles flow and leads to lower resistance deformation at increasing rates, a trend which is the opposite to that found in the CC (Figures 15a,b).

As expressed above, although dense particulate media are in general viscoplastic, dry materials show a rather frictional-dominated behavior while dense suspensions exhibit viscous-dominated response because of the viscosity of the interstitial liquid and the lubricated contacts between grains [158,159]. Interestingly, rheology of both systems can be described with a common framework by properly substituting the inertial time scale by a viscous time scale including the viscosity of the fluid phase [160]. Unsaturated wet granular media represent a different scenario, where the more or less viscous liquid forms capillary bridges. Like any thin fluid film between moving particles, the bridge generates a viscous force, which is repulsive when the particles approach or attractive when they separate, and whose magnitude increases with both liquid viscosity and interparticle velocity [124]. Moreover, the capillary force exerted by the bridge may increase the interparticle friction or decrease it, if the liquid viscosity or the deformation rate is high enough to prevent solid-solid contact [153,156,158]. Hence, there exists a complex interrelation between forces, which can be treated by means of the *capillary number* $Ca = \mu v D/\gamma \cos\theta$ (μ is the liquid viscosity and v is the rate) as the ratio of viscous to capillary forces [33]. Thus, the viscous response is more pronounced in the system when $Ca>1$. Such systems typically show increasing stress (resistance to deformation) at increasing rate, which leads to higher viscous force. Additionally, the energy dissipation due to rupture and formation of bridges between moving particles increases with both liquid viscosity and separation velocity [157], also leading to higher yield stress at faster deformation rates. Only a few studies have investigated these mechanisms causing rate dependence in unsaturated granular media containing rather large amounts of highly viscous liquids [33,156,157,187].

We propose the rate-dependent behavior of CCs to be caused by the viscous response generated by the nm-thin moisture-originated capillary bridges. As shown, an increase of both the mechanical cohesion and the viscoplastic response upon faster strain rates is observed the wet silica CC. Indeed, the expected high viscosity of confined water would justify that the thin (12 nm, and less under stress) water nanomenisci exhibit such a viscous response (but remaining fluid) to render the CC viscous flow behavior. From the analysis in the previous Section, the opal strength suggests that nanomenisci exert a viscous force larger than the capillary force, leading to $Ca > 1$. This behavior could be linked to the rate-dependent and viscous liquid-like mechanical performance of more confined water [142]. In the CC, the system viscosity reduced, from wet to dry, progressively with the amount of water. This becomes evident by representing the Δ*h* data [161] as function of the decreasing water content (Figure 19a, solid symbols), which suggests that the viscous response of the CC correlates with the volume of bridges.

Undoubtedly, the exact physical process inducing viscoplasticity must be further investigated. In order to assess the role of the nature of the particles contacts, an interesting and simple approach is investigating the rheology of CCs subjected to one-pulse CVD [161]. Thereby, the spheres are rigidly bonded by silica necks, easily providing a 'nongranular' replica for direct comparison with the original opal. The creep behavior (Figure 19) demonstrates non-viscous system response as it exhibited vanishing rate-dependence and small, slow Δ*h* (close to that of the opal at the lowest rate). Such drastically different performance compared to that of regular CCs even after dewetting shows the fundamental role of the particulate character in the system rheology. Besides, this distinction increases linearly with the degree of hydration, as the liquid bonds, contrary to rigid bridges between spheres, generate rate-dependent forces in the material. The water adsorbed on the CVD-silica of the nongranu-

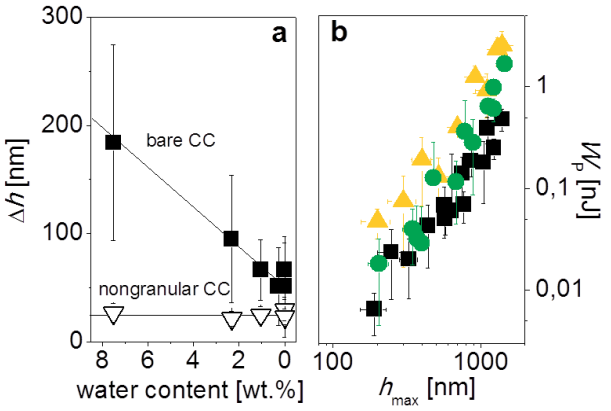

Figure 19 (a) Dependence of the creep displacement Δ*h* with the water content measured by temperature-controlled nanoindentation (load rate of 50 μN/s and dwell time of 60 s) on bare and CVD-infiltrated (nongranular) silica CCs (solid and empty symbols, respectively). Lines are linear fits. (b) Plastic work W_P measured by nanoindentation on a bare silica CC at 25 ºC and load rates of 5, 50, and 500 μN/s (black, green and orange symbols, respectively). Data in (a) are taken from Ref. 161 and represented against water content as calculated from *T* in the original experiment and using TGA from Figure 2a. (b) is adapted from Ref. 161 with permission.

lar CC (approximately in the same amount as in the regular opal) caused no rate dependence, since it does not affect the cohesion of the crosslinked (nonparticulate) ensemble. Consistently, no significant variation was measured upon removing this water by heating (Figure 19a, empty symbols). Transition from granular to nongranular behavior has also been investigated by progressively solid-bonding the CC spheres by sintering or atomic layer deposition [162].

To conclude this Subsection, a relevant aspect related to rheology in particulate materials such as energy dissipation upon (plastic) deformation must be mentioned. This is an important aspect in many practical issues, from impact absorption to digging [191,192], and it is ultimately related to the effective viscosity of the system in response to stress. In wet particulate media, capillary bridges play a central role since they not only generate friction and viscous forces but also their rupture and reformation during strain is a hysteretic, dissipative process [154,157]. In CCs, energy dissipation has been studied by means of the plastic work W_P obtained from nanoindentation, which measures the irreversible distortion of the spheres packing (Figure 15a) [161]. Figure 19b demonstrates a clear rate dependence (W_P increases one order of magnitude by rising the strain rate in two decades), which evidences the viscous nature of dissipation due to the CC nanomenisci. For sake of comparison, W_P measured in the opal is comparable to the highly absorbing polymer foams and periodic epoxy nanoframes [161]. Such performance is consistent with the most-compact packing of the CC leading to highest number of liquid necks and with the marked viscoplastic behavior exhibited by them. Along with the fact that CCs themselves may be efficient impact-absorbing materials, their controllable parameters (water content, hydrophilicity, order) can help study the role of liquid bridges in dissipative particulate media. In particular, rate-dependent system viscosity is an active research subject in colloidal and granular science [132], related e.g. to *shear thickening* (viscosity increase with shear rate), which is desirable for damping or protective materials [193] but unfavorable for many industrial processes. The opposite behavior (*shear thinning*) leads, for example, to devastating phenomena like landslides.

Micromechanics of colloidal ensembles is still practically unknown and much progress is to be done in the next future. Desirably, such advances will help understand dense granular flows in unsaturated powders and granular materials. For example, the contribution to granular rheology of highly viscous nanomenisci due to water adsorption, ignored so far, should be explored. The fact that moisture affects the mechanical response of granular materials suggests that such influence is not negligible. Powerful numerical tools for investigation of force networks and granular flows like the discrete element method have a great difficulty in assuming a distribution of the liquid, in particular, the liquid fraction forming bridges and their shape [46,172, 194]. Since these factors are achievable in silica CCs, accurate simulations can be compared to opal mechanical performance, and, in turn, it may help refine the modeling of such aspects. More generally, a better connection between macroscopic experiments used for granular-like systems and microscopic techniques like nanoindentation is needed. The fact that CCs exhibit 'granular' features points to parallelisms between the different systems irrespective the distinct scales and peculiarities. Certainly, some CC characteristics drastically differ from those of general particulate media, like the high compactness or the crystal-like structure. But even these diverging aspects can be useful if considered as extreme cases of interest, like the fcc packing related to the behavior of jammed systems. The versatile disorder degree of CCs, which is controllable from ideal fcc compacts to perfectly random assemblies (photonic glasses) [114], is an attractive advantage to study the role of parameters like coordination number or packing density, which are hardly tractable in general particulates. To what extent such parallelisms can be established must still be elucidated.

Finally, we must allude to an important case that has been not covered, namely, when the amount of wetting liquid progressively increases in the CC up to fully immersion of the spheres. The opal, then, passes from pendular to funicular state (capillary bridges begin to coalesce) until reaching *capillary* and *slurry states*, in which the gas phase is displaced by the liquid, turning into a two-phase system. The ensemble cohesion saturates at a certain point of the funicular state and drops in the binary state as the capillary action vanishes [30,31,33,36]. The exact evolution of cohesive and rheological properties of the CC throughout these regimes is of interest as it connects, on the one hand, to dense suspensions. These are an outstanding class of materials in industry and technology, ranging from paints or fresh concrete to many food products, and consequently a great effort has been made in recent years to know better their rheology. A related material, close to immersed CCs, are matrix-embedded nanocolloidal films, which are relevant for electronic and optical applications and whose micromechanical properties begin to be investigated [195]. On the other hand,

both loss of stability and drastic rheological changes may be qualitatively understood in liquid-filled granular media and soils [196] but many quantitative aspects are still not accessible [36], in spite of being of obvious interest in civil engineering or geology. Such lack of precise understanding is tragically proved by the to-date unpredictability of catastrophic phenomena like landslides [197]. The study of less-cohesive states in CCs can be an useful approach to investigate the mechanical behavior of saturated particulate media.

4. Conclusions

The understanding of the behavior of water in small environments represents an outmost complex but stimulating task in materials science and technology. In spite of the great interest for numerous aspects in both scientific and industrial fields, our knowledge of many related topics is still poor, especially those affecting particulate systems. Undoubtedly, a major difficulty is the deficit of experimental approaches to investigate liquid-solid phenomena in micro/nanometric disperse media. In view of recent advances, we have described how colloidal crystals constitute a simple, advantageous lab-on-a-chip to gain new insight into water interactions within submicron spheres assemblies. Their unique structural characteristics allow the development of original techniques that configure an incipient research area to address fundamental aspects of nanoconfined water. We have described aspects of CCs that are relevant in diverse, apparently disconnected areas at different scales, and emphasized open questions concerning all these fields that must be further explored by upcoming studies. Latest results open interesting perspectives on general wet particulate media like granular materials, which render CCs a kind of 'nano-sand' with promising utilities.

Acknowledgements

This work was partially funded by the Spanish MINECO MAT2014-58731-JIN and MAT2015-68075-R, and Comunidad de Madrid S2013/MIT-2740 (PHAMA_2.0) projects.

References

[1] Israelachvili J: Intermolecular and Surface Forces, 3rd ed. Academic Press; 2011.

[2] Rouquerol F, Rouquerol J, Sing KSW, Llewellyn P, Maurin G: Adsorption by Powders and Porous Solids: Principles, Methodology and Applications, 2nd ed. Academic; London; 2014.

[3] Yarom M, Marmur A. Vapor–liquid nucleation: the solid touch. Adv Colloid Interface Sci 2015;22:743-754.

[4] van Honschoten JW, Brunets N, Tas NR. Capillarity at the nanoscale. Chem Soc Rev 2010;39:1096-1114.

[5] Bormashenko E. Progress in understanding wetting transitions on rough surfaces. Adv Colloid Interface Sci 2015;222:92–103.

[6] Churaev NV. Surface forces in wetting films. Adv Colloid Interface Sci 2003;103:197-218.

[7] Butt HJ, Kappl M. Normal capillary forces. Adv Colloid Interface Sci 2009;146:48-60.

[8] Prokopovich P, Starov V. Adhesion models: from single to multiple asperity contacts. Adv. Colloid Interface Sci. 2011;168:210–22.

[9] Knight R., Pyrak-Nolte LJ, Slater L, Atekwana E, Endres A, et al. Geophysics at the interface: Response of geophysical properties to solid-fluid, fluid-fluid, and solid-solid interfaces. Rev Geophys 2010;48:RG4002.

[10] Ball P. Water as an active constituent in cell biology. Chem Rev 2008;108:74.

[11] Franzese G, Bianco V. Water at biological and inorganic interfaces.Food Biophys 2013;8(3):153-169.

[12] Pruppacher HR, Klett JD. Microphysics of Clouds and Precipitation, Kluwer Academic Publishers: The Netherlands, 1997.

[13] Bocquet L, Charlaix E. Nanofluidics, from bulk to interfaces. Chem Soc Rev 2010;39:1073.

[14] Tagliazucchi M, Szleifer I. Transport mechanisms in nanopores and nanochannels: can we mimic nature? Mater Today 2015;18(3):131-142.

[15] Dorfman KD, King SB, Olson DW, Thomas JD, Tree DR. Beyond gel electrophoresis: Microfluidic separations, fluorescence burst analysis, and DNA stretching. Chem Rev 2012;113(4):2584-2667.

[16] Lee J, Laoui T, Karnik R. Nanofluidic transport governed by the liquid/vapour interface. Nature Nanotech. 2014,9:317–323.

[17] Yan YY, Gao N, Barthlott W. Mimicking natural superhydrophobic surfaces and grasping the wetting process: a review on recent progress in preparing superhydrophobic surfaces. Adv Colloid Interface Sci 2011;169:80–105.

[18] Wang S, Liu K, Yao X, Jiang L Bioinspired surfaces with superwettability: new insight on theory, design, and applications. Chem Rev 2015;115(16):8230-8293.

[19] Cummings PT, Docherty H, Iacovella CR, Singh JK. Phase transitions in nanoconfined fluids: The evidence from simulation and theory. AIChE J 2010;56(4):842–848.

[20] Huber P. Soft matter in hard confinement: phase transition thermodynamics, structure, texture, diffusion and flow in nanoporous media. J Phys: Cond Matter 2015;27:103102.

[21] Mate CM: Tribology on the Small Scale: A Bottom Up Approach to Friction, Lubrication, and Wear. Oxford University Press, Oxford; 2008.

[22] Park JY, Salmeron M. Fundamental Aspects of Energy Dissipation in Friction. Chem Rev 2014;114: 677.

[23] Henderson MA. The interaction of water with solid surfaces: fundamental aspects revisited. Surf Sci Rep 2002;46:5308.

[24] Hornbaker DJ, Albert R, Albert I, Barabási AL, Schiffer P, What keeps sandcastles standing? Nature 1997;387:765.

[25] Roman-G AD, Guilbert S, Cuq B. Distribution of water between wheat flour components: a dynamic water vapour adsorption study. J Cereal Sci 2002;36:347–355.

[26] Chappuis J. A model for a better understanding of the cohesion of hardened hydraulic materials. Colloid Surf A 1999;156: 223.

[27] Hensen EJM, Smit B. Why clays swell. J Phys Chem B 2002;106:12664−12667.

[28] Frye KM, Marone C. Effect of humidity on granular friction at room temperature. J Geophys Res 2002;107:2309.

[29] Ramkrishna D: Population Balances: Theory and Applications to Particulate Systems in Engineering. Academic Press; 2000.

[30] Koos E. Capillary suspensions: Particle networks formed through the capillary force. Curr Opin Colloid Interface Sci 2014;19:575−584.

[31] Domenech T, Velankar SS. On the rheology of pendular gels and morphological developments in paste-like ternary systems based on capillary attraction. Soft Matter 2015;11:1500.

[32] Phillips KR, England GT, Sunny S, Shirman E, Shirman T, Vogel N, Aizenberg J. A colloidoscope of colloid-based porous materials and their uses. Chem Soc Rev 2016;45(2):281-322.

[33] Iveson SM, Beathe JA, Page NW. The dynamic strength of partially saturated powder compacts: the effect of liquid properties. Powder Technol 2002;127:149-161.

[34] Castellanos A. The relationship between attractive interparticule forces and bulk behavior in dry and uncharged fine powders. Adv Phys 2005;54:263–376.

[35] Herminghaus S. Wet granular matter: A truly complex fluid. World Scientific, Singapore; 2013.

[36] Mitarai N, Nori F. Wet granular materials. Adv Phys 2006; 55:1.

[37] Forterre Y, Pouliquen O. Flows of Dense Granular Media. Annu Rev Fluid Mech 2008;40:1.

[38] Khan F, Pilpel N, Ingham S. The effect of moisture on the density, compaction and tensile strength of microcrystalline cellulose, Powder Technol. 1988;54:161-164.

[39] Bocquet L, Charlaix E, Ciliberto S, Crassous J. Moisture-induced ageing in granular media and the kinetics of capillary condensation. Nature 1998;396:735–737.

[40] Ovarlez G, Kolb E, Clement E. Rheology of a confined granular material. Phys Rev E 2001;64:060302.

[41] Ravi S, Zobeck TM, Over TM, Okin GS, D'Odorico P. On the effect of moisture bonding forces in air-dry soils on threshold friction velocity of wind erosion. Sedimentology 2006;53(3):597-609.

[42] Banigan EJ, Illich MK, Stace-Naughton DJ, Egolf DA. The chaotic dynamics of jamming. Nature Phys 2013;9:288–292.

[43] Zaitsev VY, Gusev VE, Tournat V, Richard P. Slow relaxation and aging phenomena at the nanoscale in granular materials. Phys Rev Lett 2014;112(10):108302.

[44] Brown E, Jaeger HM. Shear thickening in concentrated suspensions: phenomenology, mechanisms and relations to jamming. Rep Prog Phys 2014;77:046602.

[45] Otsuki A, Bryant G. Characterization of the interactions within fine particle mixtures in highly concentrated suspensions for advanced particle processing. Adv Colloid Interface Sci 2015;226:37-43.

[46] Guo Y, Curtis JS. Discrete Element Method Simulations for Complex Granular Flows. Annu Rev Fluid Mech 2015;47:21–46.

[47] Delenne JY, Richefeu V, Radjai F. Liquid clustering and capillary pressure in granular media. J Fluid Mech 2015;762:R5.

[48] Freymann G, Kitaev V, Lotsch BV, Ozin GA. Bottom-up assembly of photonic crystals. Chem Soc Rev 2013;42:2528−2554.

[49] Gallego-Gómez F, Blanco A, López C. Exploration and Exploitation of Water in Colloidal Crystals. Adv Mater 2015;27: 2686–2714.

[50] Furumi S, Fudouzi H, Sawada T, Self-organized colloidal crystals for photonics and laser applications. Laser Photon Rev 2009;4:205.

[51] Galisteo-López JF, Ibisate M, Sapienza R, Froufe-Pérez LS, Blanco A, López C. Self-Assembled Photonic Structures. Adv Mater 2011;23:30.

[52] Bai L, Xie Z, Cao K, Zhao Y, Xu H, Zhu C, et al. Hybrid mesoporous colloid photonic crystal array for high performance vapor sensing. Nanoscale 2014;6(11):5680-5685.

[53] Fenzl C, Hirsch T, Wolfbeis OS. Photonic Crystals for Chemical Sensing and Biosensing. Angew Chem Int Ed 2014;53:3318.

[54] Nagamanasa KH, Gokhale S, Ganapathy R, Sood AK. Confined glassy dynamics at grain boundaries in colloidal crystals. Proc Natl Acad Sci 2011;108(28):11323-11326.

[55] King SB, Dorfman KD. Role of order during Ogston sieving of DNA in colloidal crystals. Anal Chem 2013;85(16):7769-7776.

[56] Gallego-Gómez F, Blanco A, Golmayo D, López C. Nanostructuring of Azomolecules in Silica Artificial Opals for Enhanced Photoalignment Adv Funct Mater 2011;21:4109.

[57] Nutz FA, Ruckdeschel P, Retsch M. Polystyrene colloidal crystals: Interface controlled thermal conductivity in an open-porous mesoparticle superstructure. J Colloid Interface Sci 2015;457(1):96-101.

[58] Gallego-Gómez F, Ibisate M, Golmayo D, Palomares FJ, Herrera M, et al. Light Emission from Nanocrystalline Si Inverse Opals and Controlled Passivation by Atomic Layer Deposited Al_2O_3. Adv Mater 2011;23:5219.

[59] Stein A, Wilson BE, Rudisill SG. Design and functionality of colloidal-crystal-templated materials—chemical applications of inverse opals.Chem Soc Rev 2013;42(7):2763-2803.

[60] Vakarelski IU, Marston JO, Thoroddsen ST. Foam-film-stabilized liquid bridge networks in evaporative lithography and wet granular matter. Langmuir 2013;29(16):4966-4973.

[61] Vogel N, Retsch M, Fustin CA, Del Campo A, Jonas U. Advances in colloidal assembly: the design of structure and hierarchy in two and three dimensions. Chem Rev 2015;115:6265–6311.

[62] Stöber W, Fink A, Bohn E. Controlled growth of monodisperse silica spheres in the micron size range. J Colloid Interface Sci 1968;26:62.

[63] Míguez H, Meseguer F, López C, Blanco Á, Moya JS, et al. Control of the photonic crystal properties of fcc-packed submicrometer SiO_2 spheres by sintering. Adv Mater 1998;10(6):480-483.

[64] Bergna HE, Roberts W O: Colloidal Silica: Fundamentals and Applications. CRC Press, Boca Raton; 2006.

[65] Gallego-Gómez F, Blanco A, Golmayo D, López C. Three regimes of water adsorption in annealed silica opals and optical assessment. Langmuir 2011;27(23):13992-13995.

[66] Labrosse A, Burneau A. Characterization of porosity of ammonia catalysed alkoxysilane silica. J Non-Cryst Solid 1997;221:107.

[67] Sacks MD, Tseng TY. Preparation of SiO_2 glass from model powder compacts: I, formation and characterization of powders, suspensions, and green compacts. J Am Ceram Soc 1984;67:526.

[68] Cho SH, Park SY, Kim C, Choi PP, Park JK. Stabilization of monodispersed spherical silica particles and their alignment with reduced crack density. Colloid Surf A: Physicochem Eng Aspects 2014;441:354-359.

[69] Nokhodchi A. Effect of moisture on compaction and compression. Pharm Tech 2005;6:46-66.

[70] Schuttlefield JD, Cox D, Grassian VH. An investigation of water uptake on clay minerals using ATR-FTIR spectroscopy coupled with quartz crystal microbalance measurements. J Geophys Res Atm 2007;112(D21).

[71] Hatch CD, Wiese JS, Crane CC, Harris KJ, Kloss HG, Baltrusaitis J. Water adsorption on clay minerals as a function of relative humidity: Application of BET and Freundlich adsorption models.Langmuir 2012;28(3):1790-1803.

[72] Yamamoto E, Kitahara M, Tsumura T, Kuroda K. Preparation of size-controlled monodisperse colloidal mesoporous silica nanoparticles and fabrication of colloidal crystals. Chem Mater 2014;26(9):2927-2933.

[73] Muldarisnur M, Marlow F. Observation of Nano-Dewetting in Colloidal Crystal Drying. Angew. Chem. Int. Ed. 2014, 53, 8761-8764.

[74] Gallego-Gómez F, Blanco A, Canalejas-Tejero V, López C. Water-Dependent Photonic Bandgap in Silica Artificial Opals. Small 2011;7(13):1838-1845.

[75] Gallego-Gómez F, Blanco A, López C. In situ optical study of water sorption in silica colloidal crystals. J Phys Chem C 2012;116(34):18222-18229.

[76] Or D, Tuller M. Liquid retention and interfacial area in variably saturated porous media: upscaling from single-pore to sample-scale model. Water Resour Res 1999;35:3591–3605.

[77] Lian G, Seville J. The capillary bridge between two spheres: New closed-form equations in a two century old problem. Adv Colloid Interface Sci 2016;227:53-62.

[78] Costanza-Robinson MS, Harrold KH, Lieb-Lappen R.M. X-ray microtomography determination of air-water interfacial area water saturation relationships in sandy porous media. Environ Sci Technol 2008;2(8):2949–2956.

[79] Scheel M, Seemann R, Brinkmann M, Di Michiel M, Sheppard A, et al. Morphological clues to wet granular pile stability. Nature Mater 2008;7:189.

[80] Fournier Z, Geromichalos D, Herminghaus S, Kohonen MM, Mugele F, Scheel M, et al. Mechanical properties of wet granular materials. J Phys: Condens Matter 2005;17: S477.

[81] Møller PC, Bonn D. The shear modulus of wet granular matter. Europhys Lett 2007; 80:38002.

[82] Rykaczewski K, Scott JHJ. Methodology for imaging nano-to-microscale water condensation dynamics on complex nanostructures. ACS Nano 2011;5:5926.

[83] Blanco A, Gallego-Gómez F, López C. Nanoscale morphology of water in silica colloidal crystals. J. Phys. Chem. Lett. 2013, 4, 1136−1142.

[84] Nagarkar SP, Velankar SS. Morphology and rheology of ternary fluid–fluid–solid systems.Soft Matter 2012;8:8464-8477.

[85] Verdaguer A, Sacha GM, Bluhm H, Salmeron M. Molecular structure of water at interfaces: Wetting at the nanometer scale. Chem Rev 2006;106:1478.

[86] MacDowell LG, Benet J, Katcho NA, Palanco JM. Disjoining pressure and the film-height-dependent surface tension of thin liquid films: New insight from capillary wave fluctuations. Adv Colloid Interface Sci 2014;206:150-171.

[87] Milchev AI, Milchev AA. Wetting behavior of nanodroplets: The limits of Young's rule validity. Europhys Lett 2001;56:695.

[88] Cheng S, Robbins MO. Capillary adhesion at the nanometer scale. Phys Rev E 2014;89(6):062402.

[89] Pakarinen OH, Foster AS, Paajanen M, Kalinainen T, Katainen J, et al. Towards an accurate description of the capillary force in nanoparticle-surface interaction. Modell Simul Mater Sci Eng 2005;13:1175−1186.

[90] Dörmann M, Schmid HJ. Simulation of capillary bridges between nanoscale particles. Langmuir 2014;30(4):1055-1062.

[91] Cheng TL, Wang YU. Spontaneous formation of stable capillary bridges for firming compact colloidal microstructures in phase separating liquids: A computational study, Langmuir 2012;28(5):2696–2703.

[92] Pashley RM, Kitchener JA. Surface forces in adsorbed multilayers of water on quartz. J. Colloid Interface Sci. 1979;71:491.

[93] Gee ML, Healy TW, White LR. Hydrophobicity effects in the condensation of water films on quartz. J. Colloid Interface Sci. 1990, 140, 450.

[94] Asay, D. B.; Kim, S. H. Evolution of the Adsorbed Water Layer Structure on Silicon Oxide at Room Temperature. J Phys Chem 2005;109:16760−16763.

[95] Garbatski U, Folman M. Multilayer adsorption on plane surfaces by capacity measurements. I. Adsorption on glass at high relative pressures.J Phys Chem 1956;60:793 .

[96] Al-Abadleh HA, Krueger BJ, Ross JL, Grassian VH. Phase transitions in calcium nitrate thin films. Chem Commun 2003;22:2796–2797

[97] Bohr J, Wogelius RA, Morris PM, Stipp SLS. Thickness and structure of the water film deposited from vapour on calcite surfaces. Geochim Cosmochim Acta 2010;74:5985–5999.

[98] Peschel G, Belouschek P, Müller MM, Müller MR, König R. The interaction of solid surfaces in aqueous systems. Colloid Polym Sci 1982;260(4):444-451.

[99] Tuller M, Or D, Dudley LM. Adsorption and capillary condensation in porous media: Liquid retention and interfacial configurations in angular pores. Water Resour Res 1999;35:1949.

[100] Tokunaga TK. Physicochemical controls on adsorbed water film thickness in unsaturated geological media Water Resour Res 2011;47:W08514.

[101] Or D, Tuller M. Liquid retention and interfacial area in variably saturated porous media: Upscaling from single-pore to sample-scale model.Water Resour Res 1999;35(12):3591-3605.

[102] Rascón C, Parry AO. Geometry-dominated fluid adsorption on sculpted solid substrates. Nature 2000;407(6807):986-989.

[103] Singha SK, Das PK, Maiti B. Thermokinetics of heterogeneous droplet nucleation on conically textured substrates. J Chem Phys 2015;143(20):204703.

[104] Kim TW, Tokunaga TK, Shuman DB, Sutton SR, Newville M, Lanzirotti A. Thickness measurements of nanoscale brine films on silica surfaces under geologic CO_2 sequestration conditions using synchrotron X-ray fluorescence. Water Resour Res 2012;48(9),W09558.

[105] James M, Darwish TA, Ciampi S, Sylvester SO, Zhang Z, et al. Nanoscale condensation of water on self-assembled monolayers. Soft Matter 2011;7:5309−5318.

[106] Giri D, Ashraf KM, Collinson MM, Higgins DA. Single-Molecule Perspective on Mass Transport in Condensed Water Layers over Gradient Self-Assembled Monolayers. J Phys Chem C 2015;119(17):9418-9428.

[107] Teschke O, Bonugli LO, de Souza EF. Anisotropic Growth of Water-Puckered Pentamers on a Mica Terrace. Langmuir 2011;28(2):1552-1561.

[108] Xu L, Lio A, Hu J, Ogletree DF, Salmeron M. Wetting and capillary phenomena of water on mica. J Phys Chem B 1998;102:540-548.

[109] Weeks BL, Vaughn MW, DeYoreo JJ. Direct imaging of meniscus formation in atomic force microscopy using environmental scanning electron microscopy. Langmuir 2005;21(18):8096-8098.

[110] Mohammadi MH, Meskini-Vishkaee F. Predicting the film and lens water volume between soil particles using particle size distribution data. J Hydrology 2012;475:403-414.

[111] Crassous J, Bocquet L, Ciliberto S, Laroche C. Humidity effect on static aging of dry friction. Europhys Lett 1999;47:562.

[112] Forcada ML. Instability in a system of two interacting liquid films: Formation of liquid bridges between solid surfaces. J Chem Phys 1993;98:638.

[113] Barcons V, Verdaguer A, Font J, Chiesa M, Santos S. Nanoscale capillary interactions in dynamic atomic force microscopy. J Phys Chem C 2012;116(14):7757-7766.

[114] Garcia PD, Sapienza R, Blanco A, López C. Photonic glass: a novel random material for light. Adv Mater 2007;19:2597.

[115] García-Santamaría F, Braun PV. Are artificial opals non-close-packed fcc structures? Appl Phys Lett 2007;90:241905.

[116] Fiscina JE, Lumay G, Ludewig F, Vandewalle, N. Compaction dynamics of wet granular assemblies. Phys Rev Lett 2010;105(4):048001.

[117] Knappenberger T, Flury M, Mattson ED, Harsh JB. Does water content or flow rate control colloid transport in unsaturated porousmedia? Environ Sci Technol 2014;48:3791–3799.

[118] Iveson SM, Page NW. The tensile bond strength developed between liquid bound pellets during compression. Powder Technol 2001;117:113– 122.

[119] Zamponi F. Packings close and loose. Nature 2008;453(7195):606-607.

[120] Juillerat F, Bowen P, Hofmann H. Formation and drying of colloidal crystals using nanosized silica particles. Langmuir 2006;22(5):2249-2257.

[121] Leng Y. Hydration force between mica surfaces in aqueous KCl electrolyte solution. Langmuir 2012;28(12):5339-5349.

[122] Sasaki S, Maeda H. Electrostatic effect on the hydration layer of colloidal silica particles. J Colloid Interface Sci 1994;167:146.

[123] Okubo T, Tsuchida A, Stoimenova M. Electro-optic effects of colloidal crystals. Adv Colloid Interface Sci 2011;162(1):80-86.

[124] Pitois O, Moucheront P, Chateau X. Liquid bridge between two moving spheres: An experimental study of viscosity effects. J Colloid Interface Sci 2000;231:26.

[125] Attard P. Nanobubbles and the hydrophobic attraction. Adv Colloid Interface Sci 2003;104:75.

[126] Peng H, Birkett GR, Nguyen AV. Progress on the Surface Nanobubble Story: What is in the bubble? Why does it exist? Adv Colloid Interface Sci 2015;222:573-580.

[127] Deb SK, Shukla MK: A review of dissolved organic matter transport processes affecting soil and environmental quality. J Environ Analytic Toxicol 1:106.

[128] Syngouna IV, Chrysikopoulos CV. Experimental investigation of virus and clay particles cotransport in partially saturated columns packed with glass beads. J Colloid Interface Sci 2015;440(15):140–150.

[129] Moscicki JK, Sokolowska D. Dehydration kinetics and conductivity scaling in time near the continuity failure of a water wetting film in granular media. Appl Phys Lett 2013;103(26):263701.

[130] Jinesh KB, Frenken JWM. Capillary condensation in atomic scale friction: how water acts like a glue. Phys Rev Lett 2006;96:166103.

[131] Major RC, Houston JE, McGrath MJ, Siepmann JI, Zhu XY. Viscous water meniscus under nanoconfinement. Phys Rev Lett 2006;96(17):177803.

[132] Schall P, van Hecke M. Shear bands in matter with granularity. Annu Rev Fluid Mech 2010;42,67-88.

[133] Hanotin C, De Richter SK, Marchal P, Michot LJ, Baravian C. Vibration-induced liquefaction of granular suspensions. Phys Rev Lett 2012;108:198301.

[134] Ishihara K. Liquefaction and flow failure during earthquakes, Geotech 1993;43:351.

[135] Soria-Hoyo C, Valverde JM, Castellanos A. Avalanches in moistened beds of glass beads. Powder Technol 2009;196:257.

[136] Bouhacina T, Desbat B, Aimé JP. FTIR spectroscopy and nanotribological comparative studies: influence of the adsorbed water layers on the tribological behaviour. Tribol Lett 2000;9(1-2):111-117.

[137] Feiler AA, Stiernstedt J, Theander K, Jenkins P, Rutland MW. Effect of capillary condensation on friction force and adhesion. Langmuir 2007;23(2):517-522.

[138] Rabinovich YI, Singh A, Hahn M, Brown S, Moudgil B. Kinetics of liquid annulus formation and capillary forces. Langmuir 2011;27(22):13514-13523.

[139] Wei Z, Zhao YP. Growth of liquid bridge in AFM. J Phys D: Appl Phys 2007;40:4368.

[140] Granick S, Bae SC, Kumar S, Yu C. Viewpoint: Confined liquid controversies near closure? Physics 2010;3:73.

[141] Li TD, Gao JP, Szoszkiewicz R, Landman U, Riedo E. Structured and viscous water in subnanometer gaps. Phys Rev B 2007;75:115415.

[142] Khan SH, Matei G, Patil S, Hoffmann PM. Dynamic Solidification in Nanoconfined Water Films. Phys Rev Lett 2010;105:106101.

[143] Kim BI, Boehm RD, Bonander JR. Direct observation of self-assembled chain-like water structures in a nanoscopic water meniscus. J Chem Phys 2013;139:054701.

[144] He M, Blum AS, Aston DE, Buenviaje C, Overney RM, Luginbühl R. Critical phenomena of water bridges in nanoasperitycontacts. J Chem Phys 2001;114:1355-1360.

[145] Contreras-Naranjo JC, Ugaz VM. A nanometre-scale resolution interference-based probe of interfacial phenomena between microscopic objects and surfaces. Nature Commun 2013;4:1919.

[146] Riedo E, Lévy F, Brune H. Kinetics of capillary condensation in nanoscopic sliding friction. Phys Rev Lett 2002;88(18):185505.

[147] Lebeau M, Konrad J-M. A new capillary and thin film flow model for predicting the hydraulic conductivity of unsaturated porous media. Water Resour Res 2010;46:W12554.

[148] Truong VK, Owuor EA, Murugaraj P, Crawford RJ, Mainwaring DE. Impact of particle nanotopology on water transport through hydrophobic soils. J Colloid Interface Sci 2015;460:61-70.

[149] Pop A, Ardelean I. Monitoring the size evolution of capillary pores in cement paste during the early hydration via diffusion in internal gradients. Cement Concrete Res 2015;77:76-81,

[150] Sakai M, van Genuchten MT, Alazba AA, Setiawan BI, Minasny B. A complete soil hydraulic model accounting for capillary and adsorptive water retention, capillary and film conductivity, and hysteresis. Water Resour Res 2015;51:8757–8772.

[151] Ali I. New generation adsorbents for water treatment. Chem Rev 2012;112(10):5073-5091.

[152] Levy A, Kalman H: Handbook of Conveying and Handling of Particular Solids. Amsterdam, Elsevier; 2012.

[153] Iveson SM, Litster JD, Hapgood K, Ennis BJ. Nucleation, growth and breakage phenomena in agitated wet granulation processes: a review. Powder Technol 2001;117:3-39.

[154] Roeller K, Blaschke J, Herminghaus S, Vollmer J. Arrest of the flow of wet granular matter. J Fluid Mech 2014;738:407-422.

[155] Ottino JM, Khakhar DV. Mixing and segregation of granular materials. Annu Rev Fluid Mech 2000;32:55–91.

[156] Xu Q, Orpe AV, Kudrolli A. Lubrication effects on the flow of wet granular materials. Phys Rev E 2007;76(3):031302.

[157] Liao C-C, Hsiau S-S. Experimental analysis of dynamic properties in wet sheared granular matter. Powder Technol 2010;197(3):222–229.

[158] Coussot P, Ancey C. Rheophysical classification of concentrated suspensions and granular pastes. Phys Rev E 1999;59:4445–57.

[159] Huang N, Ovarlez G, Bertrand F, Rodts S, Coussot P, Bonn D. Flow of Wet Granular Materials. Phys Rev Lett 2005;94:028301.

[160] Boyer F, Guazzelli É, Pouliquen O. Unifying suspension and granular rheology. Phys Rev Lett 2011;107:188301.

[161] Gallego-Gómez F, Morales-Flórez V, Blanco A, de la Rosa-Fox N, López C. Water-dependent micromechanical and rheological properties of silica colloidal crystals studied by nanoindentation. Nano Lett. 2012;12:4920.

[162] Zhang D, Zhang L, Lee D, Cheng X, Feng G. Reinforcing nanocolloidal crystals by tuning interparticle bonding via atomic layer deposition. Acta Mater 2015;95,216.

[163] Roth M, Schilde C, Lellig P, Kwade A, Auernhammer GK. Simultaneous nanoindentation and 3D imaging on semicrystalline colloidal films. Chem Lett 2012;41:1110.

[164] Raichmann Y, Kazakevich M, Rabkin E, Tsur Y. Internanoparticle bonds in agglomerates studied by nanoindentation. Adv Mater 2006;18:2028–2030.

[165] Vandamme M, Ulm FJ. Nanogranular origin of concrete creep. Proc Natl Acad Sci 2009;106(26):10552-10557.

[166] Ayouch A, Dieudonné X, Vaudel G, Piombini H, Vallé K, Gusev V, et al. Elasticity of an assembly of disordered nanoparticles interacting via either van der waals-bonded or covalent-bonded coating layers. ACS Nano 2012;6(12):10614-10621.

[167] Russell A, Schmelzer J, Müller P, Krüger M, Tomas J. Mechanical properties and failure probability of compact agglomerates. Powder Technol 2015;286:546-556.

[168] Strickland DJ, Zhang L, Huang YR, Magagnosc DJ, Lee D, Gianola DS. Synthesis and mechanical response of disordered colloidal micropillars. Phys Chem Chem Phys 2014;16(22):10274-10285.

[169] Díez-Pascual AM, Gómez-Fatou MA, Ania F, Flores A. Nanoindentation in polymer nanocomposites. Prog Mater Sci 2015;67:1–94.

[170] GDR MiDi. On dense granular flows. Eur Phys J E 2004;14:341–365.

[171] Stevens N, Tedeschi S, Powers K, Moudgil B, El-Shall H. Controlling unconfined yield strength in a humid environment through surface modification of powders. Powder Technol 2009;191(1):170-175.

[172] Soulié F, El Youssoufi M S, Cherblanc F, Saix C. Capillary cohesion and mechanical strength of polydisperse granular materials. Eur Phys J E 2006;21:349–357.

[173] Møller PCF, Bonn D. The shear modulus of wet granular matter. Eur Phys Lett 2007;80:38002.

[174] Geng J, Howell D, Longhi E, Behringer RP, Reydellet G, Vanel L, et al. Footprints in sand: the response of a granular material to local perturbations. Phy. Rev Lett 2001;87:035506.

[175] Muthuswamy M, Tordesillas A. How do interparticle contact friction, packing density and degree of polydispersity affect force propagation in particulate assemblies? J Stat Mech: Theor Exp 2006;(09):P09003.

[176] Blair DL, Mueggenburg NW, Marshall AH, Jaeger HM, Nagel SR. Force distributions in three-dimensional granular assemblies: Effects of packing order and interparticle friction. Phys Rev E 2001;63(4):041304.

[177] Yang S-H, Nosonovsky M, Zhang H, Chung K-H, Negative pressure in water capillary bridges at nanocontacts. Chem Phys Lett 2008;451:88–92.

[178] Paajanen M, Katainen J, Pakarinen OH, Foster A S, Lahtinen J. Experimental humidity dependency of small particle adhesion on silica and titania. J Colloid Interface Sci 2006;304:518.

[179] Ando Y. Effect of capillary formation on friction and pull-off forces measured on submicron-size asperities. Tribol Lett 2005;19(1):29-36.

[180] Halsey TC, Levine AJ, How Sandcastles Fall. Phys Rev Lett 1998;80:3141.

[181] Crassous J, Ciccotti M, Charlaix E. Capillary force between wetted nanometric contacts and its application to atomic force microscopy. Langmuir 2011;27(7):3468-3473.

[182] Kim H, Smit B, Jang J. Monte Carlo study on the water meniscus condensation and capillary force in atomic force microscopy. J Phys Chem C 2012;116(41):21923-21931.

[183] Wang J, Qian J, Gao H. Effects of capillary condensation in adhesion between rough surfaces. Langmuir 2009;25(19):11727-11731.

[184] Asay DB, De Boer MP, Kim SH. Equilibrium vapor adsorption and capillary force: Exact Laplace–Young equation solution and circular approximation approaches. J Adhesion Sci Technol 2010;24(15-16):2363-2382.

[185] Leroch S, Wendland M. Influence of capillary bridge formation onto the silica nanoparticle interaction studied by Grand Canonical Monte Carlo simulations. Langmuir 2013;29:12410−12420.

[186] Restagno F, Ursini C, Gayvallet H, Charlaix E. Aging in humid granular media. Phys Rev E 2002;66:021304.

[187] Yang WL Hsiau SS. Wet granular materials in sheared flows. Chem Eng Sci 2005;60:4265–4274.

[188] Schwarze R, Gladkyy A, Uhlig F, Luding S. Rheology of weakly wetted granular materials: a comparison of experimental and numerical data. Granular Matter 2013;15(4):455–465.

[189] Tegzes P, Vicsek T, Schiffer P. Development of correlations in the dynamics of wet granular avalanches. Phys Rev E 2003;67:051303.

[190] Gallego-Gómez F, Blanco A, López C. Photoinduced Local Heating in Silica Photonic Crystals for Fast and Reversible Switching. Adv Mater 2012;24:6204.

[191] Waitukaitis SR, Jaeger HM. Impact-activated solidification of dense suspensions via dynamic jamming fronts. Nature 2012;487(7406):205-209.

[192] Hosoi AE, Goldman DI. Beneath our feet: strategies for locomotion in granular media. Annu Rev Fluid Mech 2015;47:431-453.

[193] Doney R, Sen S. Ordered and Highly Scalable Granular Media for Shock Mitigation ARL-TR-3612. Army Research Laboratory; 2005.

[194] Melnikov K, Mani R, Wittel FK, Thielmann M, Herrmann HJ. Grain-scale modeling of arbitrary fluid saturation in random packings. Phys Rev E 2015;92(2):022206.

[195] Tam E, Podsiadlo P, Shevchenko E, Ogletree DF, Delplancke-Ogletree MP, Ashby PD. Mechanical properties of face-centered cubic supercrystals of nanocrystals. Nano Lett 2010;10: 2363.

[196] Boger DV. Rheology of slurries and environmental impacts in the mining industry. Annu Rev Chem Biomol Eng 2013;4:239-257.

[197] Petley, D. Global patterns of loss of life from landslides. Geol 2012;40(10):927-930.